Lab Report
S261: Optical Astronomy and Gravitational Lensing

Chenhuan Wang and Harilal Bhattarai

October 7, 2020

1. Lensing

1.1. Introduction

The Universe expands and the distance between objects increases. This is the Hubble's law [1]. A useful parameter is the Hubble parameter $H(t)$. As an important cosmological parameter, current value of Hubble parameter, or Hubble constant in short, H_0 plays an essential role in astronomy and cosmology.

Gravitational lensing is a product of general relativity. Lensing could produce multiple images of background objects. By investigating the lens images and time delay, one can determine the Hubble constant, independent of cosmological model. This is a power tool to test current model of the cosmos.

In this chapter, we try to determine the Hubble constant with this method. First off, some key theoretical backgrounds are introduced. Then the whole procedure of observations and analysis will be presented.

1.2. Background

1.2.1. Cosmic Expansion

A spatially homogeneous and isotropic Universe can be described as FLRW metric. Solving Einstein's field equations with FLRW metric gives expansion of the Universe [2]. Hubble parameter $H(t) = \dot{a}(t)/a(t)$ evolves according to

$$H^2(t) = H_0^2 \left[\Omega_{\mathrm{rad}} a^{-4}(t) + \Omega_{\mathrm{mat}} a^{-3}(t) + \Omega_{\mathrm{curv}} a^{-2}(t) + \Omega_\Lambda\right] \tag{1.1}$$

Because of expansion of the Universe, light emitted in the past gets redshifted over time. The redshift of a source is given by,

$$z = \frac{\lambda_{\mathrm{obj}} - \lambda_{\mathrm{em}}}{\lambda_{\mathrm{em}}} \tag{1.2}$$

Where, λ_{obs} and λ_{em} are, respectively, the wavelengths at time of observation and emission. Redshift is directly related to the scale factor by,

$$1 + z = \frac{1}{a(t_{em})} \tag{1.3}$$

with scale factor at present time defined as $a(t_0) = 1$. Also, this equation shows that the Universe was half of its current size when a source at redshift $z = 1$ is observed.

The local Hubble law is given by the following formula,

$$v_{\mathrm{esc}} = H_0 D \tag{1.4}$$

where, $H_0 = H(t_0)$ is Hubble constant and D is the distance between object and observer.

1.2.2. Distances

Accordingly, one defines the angular diameter distance as exactly this ratio,

$$D_{\mathrm{ang}}(z) = 2R/\delta = a(z) f_K(w) \tag{1.5}$$

Where, R is the radius of the distant object, δ is the angular diameter, and z is the cosmological redshift. If we consider an observer at redshift z_1 gives the angular diameter of another object at redshift z_2, so equation 1.5 becomes [3]

$$\begin{aligned} D_{\mathrm{ang}}(z_1, z_2) &= a(z_2) f_K[w(z_2) - w(z_1)] \\ &= \frac{1}{1+z_2} f_K \left[\frac{c}{H_0} \int_{z_1}^{z_2} \frac{\mathrm{d}z'}{\sqrt{(1-\Omega_{\mathrm{m}}-\Omega_\Lambda)(1+z')^2 + \Omega_{\mathrm{m}}(1+z')^3 + \Omega_\Lambda}} \right] \end{aligned} \tag{1.6}$$

1.2.3. Quasars

Quasars (QUASi-stellar radio sources) are an extremely luminous and distant active galactic nuclei (AGN). The power for AGNs comes from accretion of matter onto super-massive black-hole, where the significant fraction of the gravitational energy is released as radiation. The radiating part of the quasars must be very compact due to the variability nature [3]. Quasars have variable luminosity at shorter wavelength which can be used to determine the time delay between light beams.

1.2.4. Gravitational lensing

A gravitational field is caused by distribution of the matter like, a cluster of galaxies between distant light source and an observer. Due to the effects of this field, light rays are bending traveling from a source to an observer. This effect is called the *gravitational lensing*. The general situation of gravitational lensing is considered as in figure.1.1 Where, we suppose the mass distribution at distance $\mathrm{D_d}$, a source is located at distance $\mathrm{D_s}$, and $\mathrm{D_{ds}}$ is the distance from deflector to a source. All distances used in gravitational lensing are the angular diameter distances.

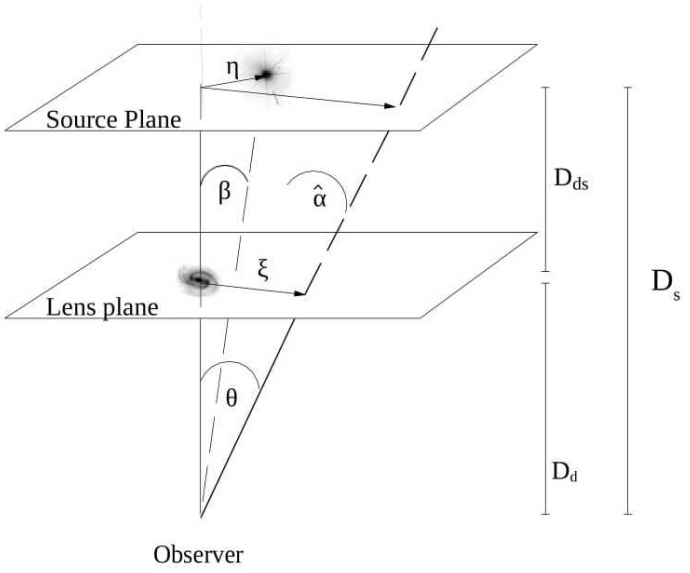

Figure 1.1.: schematic diagram of a gravitational lensing [3].

Lens Equation

To study the deflection of light by mass distribution, called lens system, we consider some conditions. First, the distance from an observer to lens and lens to a source is very large so we assume that all angles considers are small i.e. $\tan x \approx \sin x \approx x$. Secondly, source plane and lens plane are parallel, and deflection of light only occur in lens plane as in Born approximation. For a given source, the lens equation is given by,

$$\boldsymbol{\beta} = \boldsymbol{\theta} - \boldsymbol{\alpha}(\boldsymbol{\theta}) \tag{1.7}$$

where, $\boldsymbol{\theta}$ is the apparent angular position of the source in the sky, $\boldsymbol{\beta}$ is its true position, and $\boldsymbol{\alpha}$ is the scaled deflection angle.

The scaled deflection angle and true deflection angle are connected as,

$$\boldsymbol{\alpha}(\boldsymbol{\theta}) = \frac{\mathrm{D_{ds}}}{\mathrm{D_s}}\hat{\boldsymbol{\alpha}}(D_d\boldsymbol{\theta}) \tag{1.8}$$

Now, we can define a dimensionless surface mas density with convergence as,

$$\kappa(\boldsymbol{\theta}) = \frac{\sum(D_d\boldsymbol{\theta})}{\sum_{\mathrm{cr}}} \tag{1.9}$$

with the critical surface mass density,

$$\Sigma_{\mathrm{cr}} = \frac{c^2}{4\pi G}\frac{D_s}{D_d D_{ds}} \tag{1.10}$$

The scaled deflection angle can be written purely in terms of observable angles as,

$$\boldsymbol{\alpha}(\boldsymbol{\theta}) = \frac{1}{\pi}\int \mathrm{d}^2\theta'\,\kappa(\boldsymbol{\theta}')\frac{\boldsymbol{\theta}-\boldsymbol{\theta}'}{|\boldsymbol{\theta}-\boldsymbol{\theta}'|^2} \tag{1.11}$$

For further convenience, a deflection potential is introduced

$$\psi(\boldsymbol{\theta}) = \frac{1}{\pi} \int \mathrm{d}^2\theta' \, \kappa(\boldsymbol{\theta'}) \ln |\boldsymbol{\theta} - \boldsymbol{\theta'}| \tag{1.12}$$

The use of this quantity is well-motivated because it encloses all information of the mass distribution of the lens [3]. In addition, relation of deflection potential and deflection angle can be found

$$\boldsymbol{\alpha}(\boldsymbol{\theta}) = \boldsymbol{\nabla}\psi(\boldsymbol{\theta}) \tag{1.13}$$

From the deflection potential a further scalar function, the Fermat potential, can be defined

$$\tau(\boldsymbol{\theta};\boldsymbol{\beta}) = \frac{1}{2}(\boldsymbol{\beta} - \boldsymbol{\theta})^2 - \psi(\boldsymbol{\theta}) \tag{1.14}$$

Finally to find the magnification of the images is given by

$$\mu = (\det A)^{-1} \tag{1.15}$$

where, A is the Jacobian matrix of lens mapping.

$$A_{ij} = \frac{\partial \beta_i}{\partial \theta_j} \tag{1.16}$$

Strong lensing

Multiple images of a source can be obtain in strong lensing. It can be describe by considering the Format potential $\tau(\boldsymbol{\beta};\boldsymbol{\theta})$ with fixing β and assuming $\det A \neq 0$ [3].

- Minima: $\det A > 0$, tr $A > 0$
- Maxima: $\det A > 0$, tr $A < 0$
- Saddle points: det $A < 0$

Critical curves and Caustics: Those points in image plane where the magnification diverges i.e. det $A = 0$ called critical curves. Also, the mapping of a critical curve into the source plane is called caustics. In general, critical curves are closed and smooth. Caustics are closed, but not necessarily smooth.

The Odd Number Theorem

If a source has a large offset from line of sight from observer to the lens, it is easy to see only one image. The odd number theorem tells us, when we started with one image there will always be an odd number of images of gravitational lensing; however, normally at least one of them is highly de-magnified. So, we can only observe even number of images mostly as doubly or quadruply [3].

The SIS (Singular Isothermal Sphere)

A simple model to describe the mass distribution of a galaxy acting as a lens is the singular isothermal sphere (SIS):

$$\rho(r) = \frac{\sigma_v^2}{2\pi G r^2} \tag{1.17}$$

where σ_v is the velocity dispersion. Physically this means that the lens system consists of self-gravitating with Maxwellian velocity distribution [4].

Integration along the line of sight yields the surface mass density

$$\Sigma(\xi) = \frac{\sigma_v^2}{2G\xi} \tag{1.18}$$

A characteristic angular scale of an axisymmetric lens is given by the Einstein radius θ_E , defined as the angle inside which the mean of the convergence is unity. As a consequence, the projected mass inside θ_E can be written as [3],

$$M(\theta \leq \theta_E) = \pi \theta_E^2 D_d^2 \Sigma_{cr} \tag{1.19}$$

We use it to determine the mass of the lensing galaxy. For an SIS the Einstein radius can be calculated as [3],

$$\theta_E = 4\pi \left(\frac{\sigma_v}{c}\right)^2 \frac{D_{ds}}{D_s} \tag{1.20}$$

1.2.5. Time Delay

We have described about multiple images on the topic strong lensing. Light rays of different images have different paths from source to observer, thus there can be different travel times. There are two different contributions of time delay. First one is geometric time delay and second is the potential time delay which induced by the way of light through a gravitational potential [3].

We will find the time delay by using the following expression [3]

$$c\Delta t(\beta) = (1 + z_{\rm d}) \frac{\rm D_d D_s}{\rm D_{ds}} [\tau(\boldsymbol{\theta}_{\rm A}; \boldsymbol{\beta}) - \tau(\boldsymbol{\theta}_{\rm B}; \boldsymbol{\beta})] \tag{1.21}$$

here, $\boldsymbol{\theta}_{\rm A,\ B}$ are the positions of the two images. Equation 1.21 shows that the time delay is proportional to the inverse Hubble constant, i.e.

$$\boldsymbol{\Delta} t \propto \frac{1}{\rm H_0} \tag{1.22}$$

In this experiment we can use *minimum dispersion method* to calculate time-delays. The light curve for one quasar image is denoted as $A(t_k)$ and other one is $B(t_k)$ which is shifted by time shift λ. In this case, the dispersion function $\rm D^2$ is defined as [3],

$$\rm D^2(\lambda, \Delta m) = \sum_{k=1}^{N} (A(t_k) - B(t_k + \lambda, \Delta m))^2 \tag{1.23}$$

where the light curves are sampled at a discrete number of times t_k and Δm is the magnitude shift. This method basically search for minimal dispersion in 2d-plane of λ and Δm. The error bars of the time delay can be estimated by a Monte-Carlo strategy.

1.2.6. Calibration frames

In astronomical observation, the different kind of calibration frames are necessary for image reduction. These frames are described as following.

BIAS

An empty CCD (Charge Coupled Detector) has still get positive numbers due to DC offset that is added in the electronics and A/D converter. In addition there is read out noise present. This is called bias [3]. A BIAS frame is obtained by taking exposure of no exposure time with shutter closed and the image read out of unexposed CCD.

DARK

The main purpose of dark frame is to measure the dark current (thermal noise). The dark frames are made by taking expose time equal to the largest exposure time of science frame with shutter closed [3].

FLAT

All the pixels of CCD have different quantum efficiency (QE), so they need to be properly normalized. One way to obtain a flat field frame is by illuminating the telescope dome from the inside and taking short exposures as not to saturate the CCD. It is called dome flats and they can always obtain even during daytime. Another way is by sky flats which are obtained by taking exposures during evening and/or morning twilight [3].

1.2.7. Image reduction

The image reduction is done to remove instrumental signature and improve the signal-to-noise (S/N) in the data before extracting any scientific information[3].

Super-flat and Fringing

If the flat frame unable to flatten the pixels properly then we should use super-flat. The position of the telescope is slightly displaced every time, dithering, to avoid the same region of the sky falling on to the pixels. It also correct the falling of important data on bad pixels in the image. Science exposures should be used for a super-flat frame [3].

If the variations in the science frame are multiplicative, then the science frame have to be divided by the supper-flat. However, if the variation are additive, then we get a fringe pattern which is subtract by de-fringing model. These fringes mainly occur on a CCD image from monochromatic light due to interference. Since fringing is an additive effect so it must be subtracted from the science frame. Fringe model is obtained by smoothing the super-flat with large number of pixels and subtracted from the science images to obtain fully corrected images for pixel-to-pixel variations [3].

Masking and Weighting

During the analysis of data, bad pixels cause problems that lead incorrect result. It can be assigning these pixels by a certain value. Then these values recognised by the software

programs and neglect them. The mask file contain information about the exposure time which turns them into weight image [3].

Astrometric Calibration

The mapping between image co-ordinate and sky co-ordinate. It should done with the help of catalog, so we use reference catalog on-line (SDSS-R9). Then the astrometric solution is calculated by using Scamp software package [3].

Sky Subtraction

Along with the target object CCD also collects light from background sky. This has to be removed from the image to get only the flux from the object of interest. To do so, first, we have to remove all the objects in the frame and image has to be smoothed with a specific kernel width. The background image is subtracted from the original frames [3].

Co-adding

Stacking all science frame in to one master frame is called Co-adding. One needs to make sure that each objects should fall onto the same pixel. This leads to the high S/N values than individual frames [3].

Photometric Calibration

The earth atmosphere play an important role in our observations. Different telescopes have different flux values for the same target in different atmospheric conditions. For standard stars, the relation between instrumental magnitude and true magnitude is given by [3],

$$m_{\text{calb}} = m_{\text{instr}} + Z \tag{1.24}$$

where Z is the photometric zero point.

1.3. Preparatory Tasks

Calculation of the deflection potential $\psi(\theta)$ and the scaled deflection angle of an SIS lens. From equation 1.12 the deflection potential, which gives the information about the mass distribution of the lens, is define as,

$$\psi(\theta) = \frac{1}{\pi} \int d^2\theta' \kappa(\theta') \ln|\theta - \theta'| \tag{1.25}$$

In the case of axial symmetry of SIS lens equation 1.12 simplifies to (given in the question)

$$\psi(\theta) = 2 \int_0^{\theta} d\theta' \theta' \kappa(\theta') \ln\left(\frac{\theta}{\theta'}\right) \tag{1.26}$$

By substituting the values of $\Sigma(D_d\theta)$, where $D_d\theta = \xi$ from equation 1.18 and Σ_{cr} from equation 1.10 and equation 1.9, then by plugging the new expression of $\kappa(\theta)$ equation 1.26 becomes

$$\psi(\theta) = \frac{4\pi}{c^2} \frac{D_{ds}}{D_s} \sigma_v^2 \int_0^{\theta} d\theta' \ln\left(\frac{\theta}{\theta'}\right)$$

Therefore for $\theta > 0$,

$$\psi(\theta) = \theta_E \theta \tag{1.27}$$

From equation 1.13 scaled deflection angle is defined as

$$\alpha(\theta) = \nabla\psi(\theta)$$

From equations: 1.27 and 1.3,

$$\alpha(\theta) = \nabla\theta_E\theta = \theta_E \frac{\theta}{|\theta|} \tag{1.28}$$

Solving the lens equation and finding the separation between images
The lens equation in axial symmetric case can be written as

$$\beta = \theta - \alpha(\theta)$$

By using the expression for scaled deflection angle for SIS from 1.28

$$\beta = \theta - \theta_E \frac{\theta}{|\theta|}$$

There are two solutions ($\theta/|\theta| = \pm 1$)

$$\theta_{A,B} = \beta \pm \theta_E \tag{1.29}$$

Thus, the separation of these images is given by

$$\Delta\theta = \theta_A - \theta_B = 2\theta_E \tag{1.30}$$

Magnification ratio of the two images of SIS lens.
The determinant can be computed with equation 1.29 by

$$\det \mathcal{A} = \frac{\beta}{\theta}\frac{\mathrm{d}\beta}{\mathrm{d}\theta} = \begin{cases} 1 - \frac{\theta_E}{\theta_A} & \text{for A} \\ 1 + \frac{\theta_E}{\theta_B} & \text{for B} \end{cases} \tag{1.31}$$

The magnification of a gravitational lens is given by equation 1.15. If one assume the ratio of magnification is the ratio of flux, then image A has more flux coming in. The flux ratio of two images is

$$\left|\frac{\mu_A}{\mu_B}\right| = \frac{\theta_A}{\theta_B} \tag{1.32}$$

Time delay derivation for SIS lens as a function of θ_A and θ_B.
Plugin the solution in equation 1.21 and also taking care of negative image, we have

$$c\Delta t_{\mathrm{SIS}} = \frac{1}{2}(1 + z_d)\frac{D_d D_s}{D_{ds}}(\theta_A^2 - \theta_B^2) \tag{1.33}$$

Minimum Dispersion Estimator
Minimum dispersion method as described before assume the functional form of light curves is sufficiently smooth, so that the function in between the increments of λ and Δm can be properly interpolated. One way to deal with this, is to explore the whole 2d plane of $D^2(\lambda, \Delta m)$.

The approximation of dispersion function near the minimum by a parabola.
The dispersion function near the minimum can be found by Taylor expanding equation 1.23

$$D^2(\lambda) = D^2(\lambda_0) + \frac{\mathrm{d}D^2(\lambda_0)}{\mathrm{d}\lambda}(\lambda - \lambda_0) + \frac{\mathrm{d}^2D^2(\lambda_0)}{\mathrm{d}\lambda^2}(\lambda - \lambda_0)^2 + \mathcal{O}\big((\lambda - \lambda_0)^3\big) \tag{1.34}$$

The dispersion function is minimum at $\lambda = \lambda_0$. So the second term of equation 1.34 goes to zero.

1.4. Image reduction

Calibration frames and science frames have been already taken. Dark frames are not provided and not necessary, since dark currents can be neglected in this case due to proper cooling. Here these images will get inspected and reduced as explained in section 1.2.7.

1.4.1. Raw-image inspection

Calibration images are firstly visually inspected using `ds9` with `zscale` setting. Figure 2.3 and 1.2b are examples of bias and flat frames. In total, there are 10 bias frames and 9 flat frames.

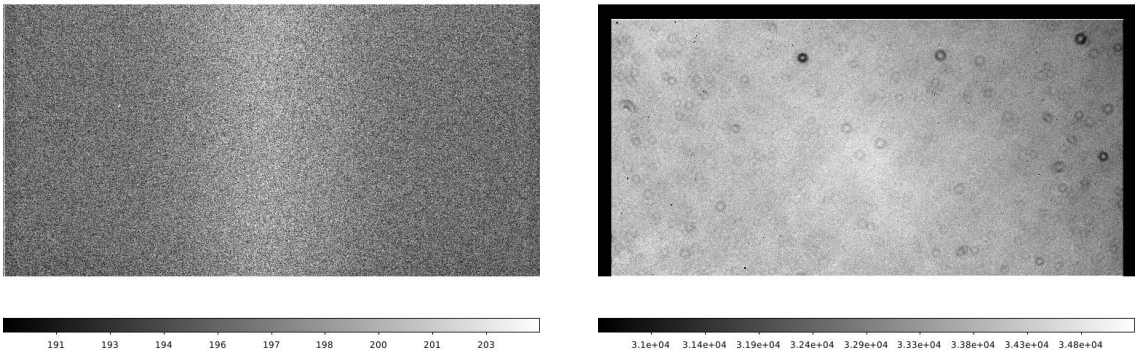

(a) Bias frame

(b) Flat frame.

Figure 1.2.: Calibration frames.

Average bias level is somewhat near 200. This values changes, though not so obvious in figure 2.3, throughout the image. Left and right sides are significantly darker, meaning less bias. Presumably it is related to geometry and layout of CCD chip. Sometimes one can see quite large white dots in bias picture. Positions of these white dots vary from image to image. Because of its significant size comparing to other noises, they are mostly likely to be cosmic rays, as hinted by [3].

Middle of bias frame is chosen to calculated background and sigma, since it doesn't have large-scale variation. Output of `imstats` gives us mean and sigma: 198.72 ± 2.59. Noise here should be readout variations and random fluctuations [3].

In flat-field, most obvious feature is black circles or doughnuts. These are dusts on dewar windows and/or filter [3]. This results in lower photon counts, thus black in flat-field images. They are not on CCD chips, since they are not properly focused. Some large-scale structure can be seen. It can be explained by different quantum efficiency at different area of CCD. There are quite a lot small sharp black dots visibly. They are most likely to be bad pixels and dust directly on CCD chip.

Each flat-field has different exposure time. One can try to find correlation between mean value of image and exposure time using commands provided in [3]. Ratios between these two goes down with increasing exposure time. Firstly of all, CCD chips should not be saturated here, since with exposure time, mean values goes down. One possibility is that read-out noise in circuit gets averaged out with long exposure time, thus lower ratio. Shot noise should play a

more important role here. It becomes especially the (one of) dominate noises at long exposure time.

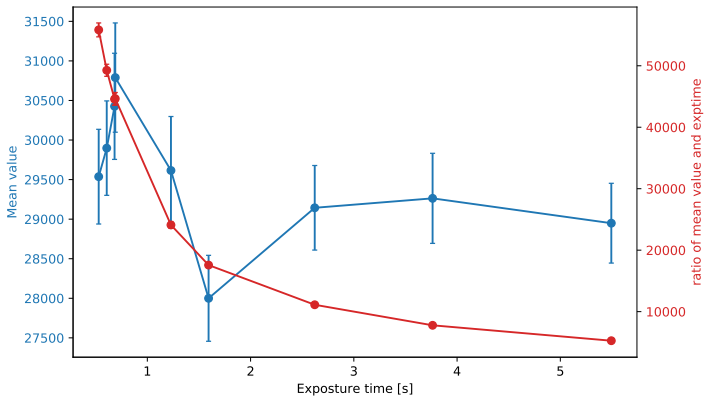

Figure 1.3.: Mean values (red) with sigmas and the ratios (blue) against exposure time of flat-field images.

In science frame one can clearly see doughnut structures and sharp black dots as in flat-field frames. Between exposure, most out-standing change would be that telescope is moving around.

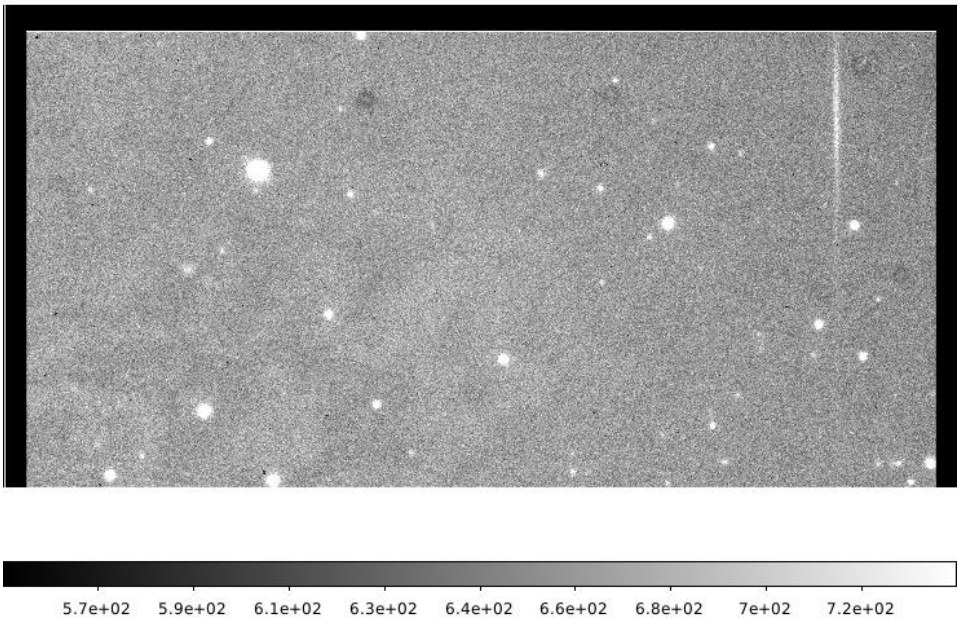

Figure 1.4.: An example of science frame.

We use `image008068.fits` as an example and compute mean and sigma in area without bright objects. Values are 693.20 ± 19.00. It is greater than the mean value of bias frame. This is easy to understand, since science frame must contain sky. And average pixel count in flat frames is significantly larger than in bias.

1.4.2. Image reduction

Several science frames containing source `SDSS1650+4251` are taken from one filter (R). Now these images with be reduced with help of calibrations frames and some more in `theli`. `theli` mainly consists of several tabs or processing groups. Each of following paragraph corresponds one processing group/

Initialise First off, `theli` should be properly reset and initialised. Number of CPU cores and instrument (telescope) are specified accordingly. Paths to image files containing bias, flat, and science frames are filled in.

Preparation Through this processing group, headers contained in `.fits` files can be split and/or corrected. Comparison of headers before and after corrections reveals

- size in x and y are swapped, meaning orientations of images have been changed,
- (useless) information, e.g. comments, CCD info, Date, and etc. have been removed,
- lots of lines starting with `DUMMY` have been added.

They are more changes, but the listed alterations are most noticeable.

Calibration In this step, calibration frames are getting co-added. In co-addition process, images are stacked on top of each other, while making sure each object falls onto the same pixel [3]. By doing this and in the end only calibrating with co-added images, random noises will get averaged out.

After co-addition, bias frames are free of small white dots as seen before and flat frames get a bit brighter. One can further computer noise dispersion of co-added bias frame and single bias frame. They are respectively 0.72 and 2.27. So noise level in co-added images is much lower.

The minimal value in normalised flat-field is 0. Dithering during co-addition helps to remove bright objects (stars and etc.).

Background modelling In this processing group, only background model correction is selected, where a super-flat and fringe model is created and applied. Its configurations are set according to [3]: `DT` = 1.0, `DMIN` = 10, mask expansion factor= 3, `median` combination, `divide smoothed model, subtract fringes` method, smoothing kernel for background model = 256.

In super-flat, one can clearly see fringes pattern. Fringes and background sky can be extracted with smoothing process. In `SDSS1650+4251_R_block0_1_fringe.fits`, there is only fringes visible and in `SSD1650+4251_R_block0_1_illum.fits` only smooth gradient, i.e. background.

Correction given by illumination is roughly 500 (counts). Fringes are removed after correction, see figure 1.5a and 1.5b.

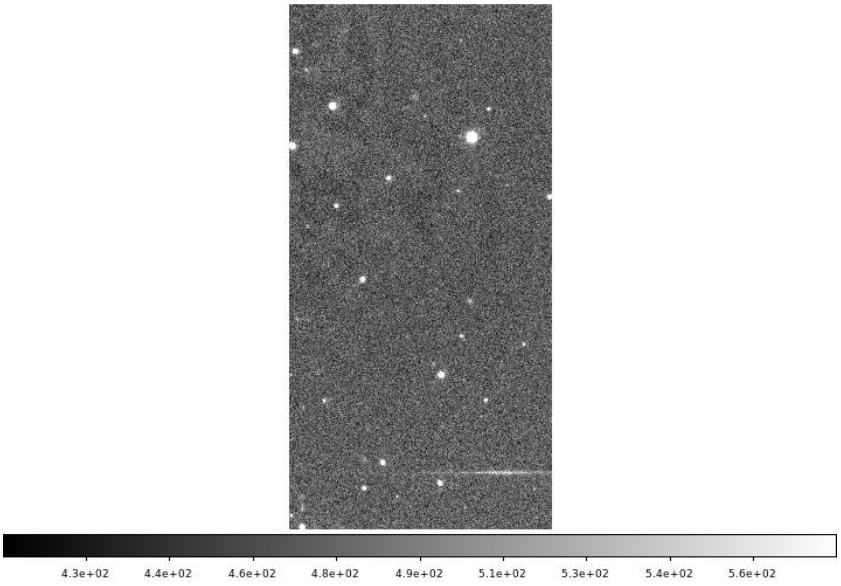

(a) Before correction. Pay attention to top left corner.

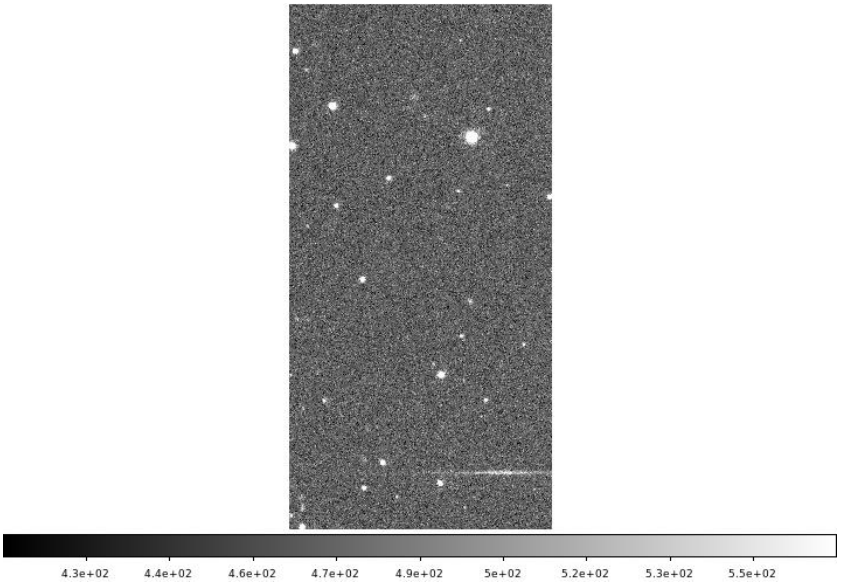

(b) After correction. Pay attention to top left corner.

Figure 1.5.: Background modelling

Weighting In this step, weighting and masking are performed to compensate bad pixels and different quantum efficiency. Global weights and WEIGHTS are created and applied.

Astrometry/Photometry This processing group matches dithered frame to standard astrometric coordinates and performs photometry calibration. Astrometric reference catalog is retrieved using setting provided in [3]: `Web(france)`, `SDSS-DR9`, `mag limit9|`, `radius=5'`. 421 objects are found. Then detection threshold is set to 2σ and minimal area for detection of

10 pixels.

Matching is done with `Scamp` with `DISTORT_DEGREES=1`. Calculation is done after `Scamp` has been correctly configured. After this, numerous check plots are generated.

Co-addition Frames are astrometrically co-added, subtracted by sky/background, and normalised to exposure time of 1 s. Settings are again provided in [3]: `Model the sky`, `DT=1`, `DMIN=10`, `kernel width=256`, outlier rejection to 4. After co-addition, newly generated frames can be found in new folder with name starting with `coadd_`, see figure 1.6. Logically, they have the same shapes and brightest region of co-added weight frame also has high S/N ratio. Indeed, one can compute noise using `imstats` as before. RMS of region free off bright objects is 0.02, far lower than previous single frames. This can be properly understood, since frames are co-added and then normalised, resulting high S/N ratio.

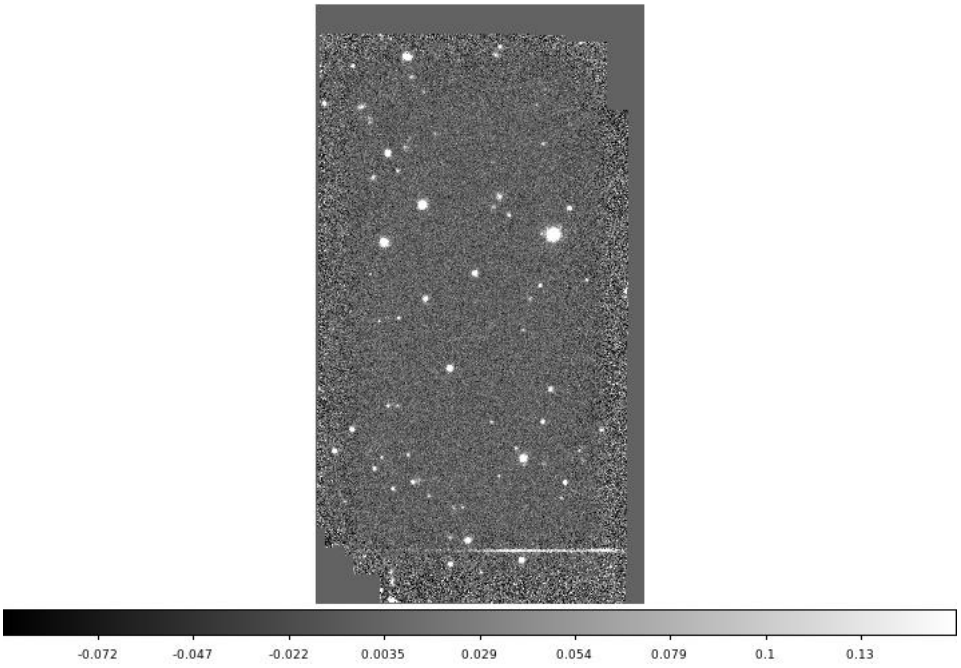

(a) Co-added frame

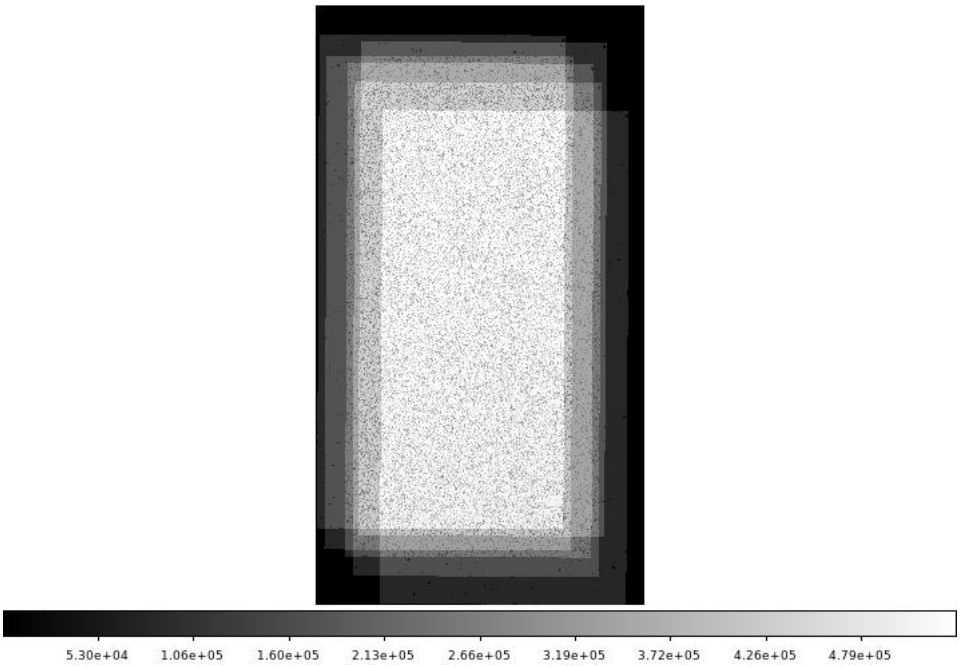

(b) Co-added weight

Figure 1.6.: Frames generated after co-addition

1.5. PSF extraction

In this section, point-spread-function (PSF) will be extracted. First of all, the target need to be found using standard coordinates: RA = $16^{h}50^{m}43.4^{s}$, DEC = $+42°51'49''.00$. In `ds9`, coordinates can be turned on with `coordinate grid` option, see figure 1.7. As mentioned in [3], this target consists of two lensing images, but the separation is similar to a typical seeing, so images are blended.

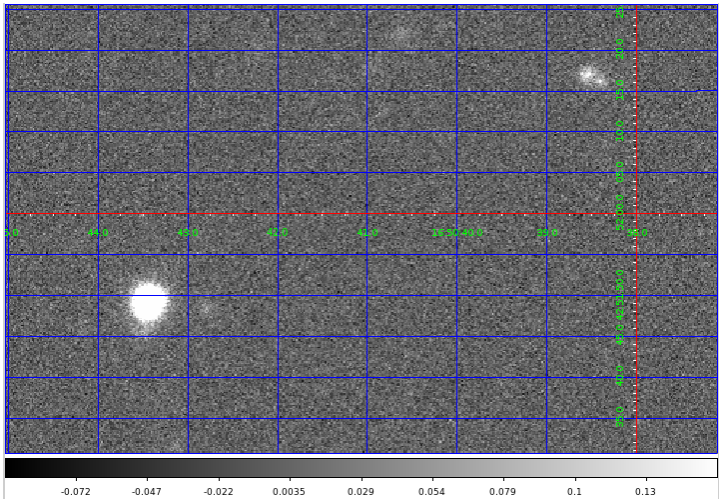

Figure 1.7.: Co-added frame with coordinate grid. Target is the left-bottom bright object.

In order to perform component fitting, PSFs of other various objects need to be extracted. One can gain more detailed information about objects using `iraf` task `imexam`.

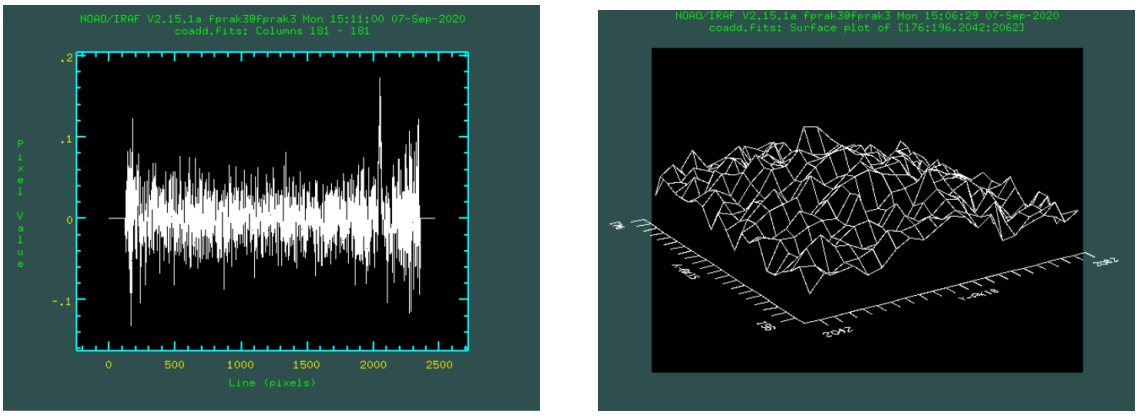

(a) Column plot

(b) Surface plot

Figure 1.8.: Example plots of a galaxy

There are mainly two categories of objects: stars and galaxies. Since galaxies contain a number of radiation sources, their full widths at half maximum (FWHMs) are typically larger than single stars. Indeed, that is what we see. FWHMs of stars are $\sim 6 \pm 1$ pixels, of galaxies $\sim 9 \pm 1$ pixels. Identification of stars and galaxies can be easier with various plots provided by

`imexam`. Two example plots each are figure 1.8 and 1.9. In contour plots, stars appear to be (almost perfect) concentric circles while galaxies are messier. Radial profiles of star have clear trend while they are scattered for galaxies. These plots support previous argument regarding differentiation stars from galaxies.

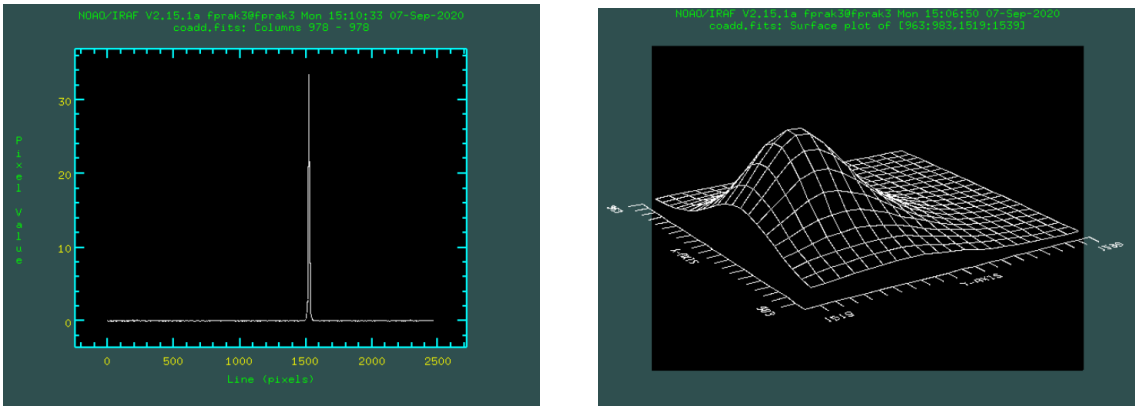

(a) Column plot (b) Surface plot

Figure 1.9.: Example plots of a star

One can try to determine the seeing of the instrument using the images of stars, since they are ideally point sources. Here all of the stars in appendix A.1 are used (of course except the last one, which is the quasar images). Given the information that 1 pixel is $0''.177$ from [3], the seeing is

$$8.04 \pm 0.11 \text{ pixels} = 1''.42 \pm 0.02 \tag{1.35}$$

Target contains two images, so its FWHM lies in between stars and galaxies at 8.71 pixels. Plots of target appear a bit different as well, see figure. 1.10. While surface plot do have some rough edges, column plot gives us a hint that this objects contains two images.

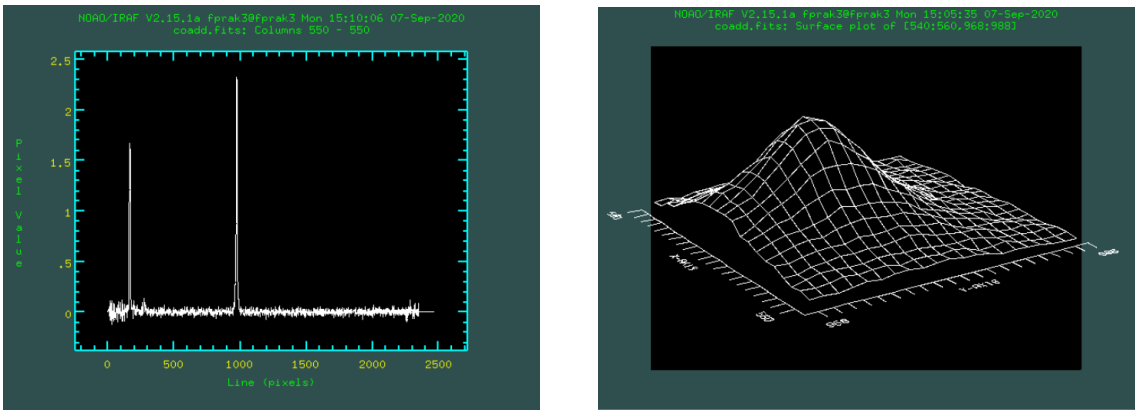

(a) Column plot (b) Surface plot

Figure 1.10.: Example plots of the target

Now to extract PSFs, a `csh` shell script `create_psf.csh` is used. The script takes four

inputs: `DIR` the directory containing the images, `LIST` containing outputs of `imexam` of selected stars and the target, `Radius` size of square getting cut, and `MAX_FWHM_STACK` the maximal size of PSF. One needs to use stars, since they are quasi-point-like sources. Stars brighter (higher flux) than the target need to be included in `LIST`. `RADIUS` is set to 30 pixels and `MAX_FWHM_STACK` to 8.5. `LIST` file can be found in A.1.

Outputs of `create_psf.csh` are each individual cut-outs `cut_scale*.fits` and stacked PSF `cut_star_stack_scale.fits`. Inspection of `cut_star_stack_scale.fits` shows that there is no contribution from neighbouring stars, see figure 1.11b. MFWHM of the stacked image is 8.09 as expected. Its surface plot is quite a smooth hump, even smoother than the hump of a single star. In the subsequent component fitting, the stacked image will be used, since all fluctuations/errors are averaged out.

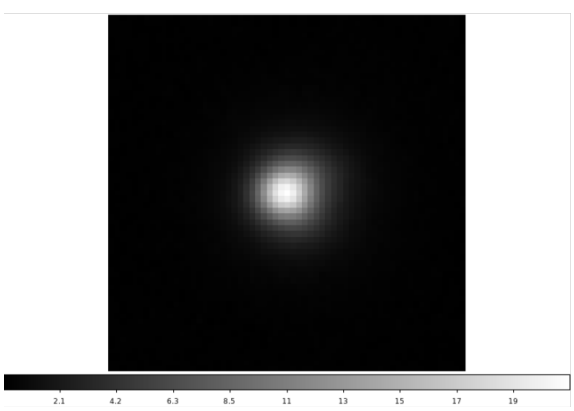

(a) The Stacked image in ds9

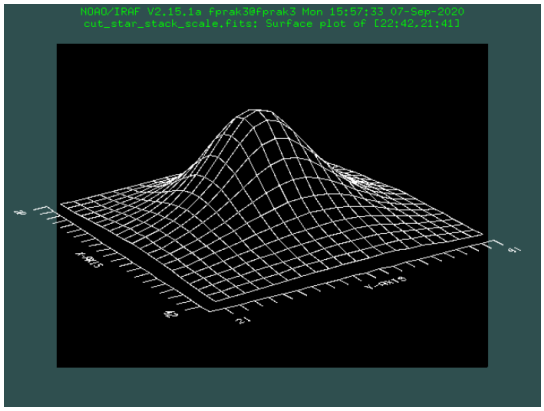

(b) Surface plot of stacked image

1.6. Component fitting

Although two images are blended, one can still try to use component fitting to find out individual flux and their separation. The 2d fitting program `galfit` is used here.

`galfit` is able to fit sky value in images and sky background is important to compute the σ-image [5]. Sky value is a fit parameter in `galfit`, thus one need to compute it using `imstats` and `dfits` for normalisation: sky=1.71 s^{-1}. This value is then added into the image with `ic` command provided in [3].

Input parameters of fitting are stored in `galfit.input`, listed in appendix. A.2. Most important things are positions of two images and relative magnitude. These are just rough estimates as initial guess. Sky background is the third component of the fitting and sky ADU counts from previous part are given as input.

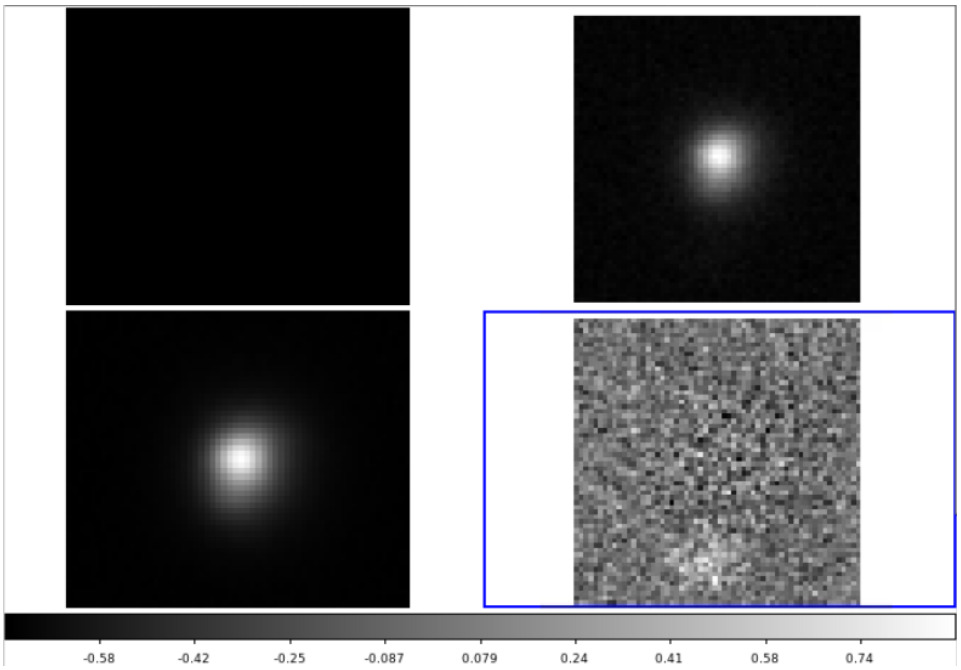

Figure 1.12.: The image block generated by galfit assuming there are *two* images. First image is intended to be empty. Second and third are respectively original and modelled images. Last one shows the residuals.

Execution of component fitting with the given parameter list outputs a log file `fit.log` shown in appendix A.3 and a image block, see figure 1.12. The log file contains the coordinates of two images

$$\begin{aligned} \boldsymbol{r}_A &= (31.11 \pm 0.01, 31.16 \pm 0.01) \\ m_A &= 17.50 \pm 0.00 \\ \boldsymbol{r}_B &= (29.69 \pm 0.05, 24.71 \pm 0.08) \\ m_B &= 19.20 \pm 0.02 \end{aligned} \tag{1.36}$$

and $\chi^2_\nu = 44.542$. From the residuals, one can see that the fitting works properly. They are quite uniformly distributed with some fluctuation, except there is a slightly bright spot at bottom. As suggested by the tutors, it could be caused by neighbouring stars.

One could also wonder if the target could consist only of one image, since it appears to be so visually. Another fitting is done but only with two components, one PSF fit and one sky background. Content of the log file can be found in appendix A.3. Resultant image block is figure 1.13. There is a clear dark spot in the residual plot and $\chi^2_\nu = 101.615$, much worse than previous fitting. So the image cannot be explained by just one image.

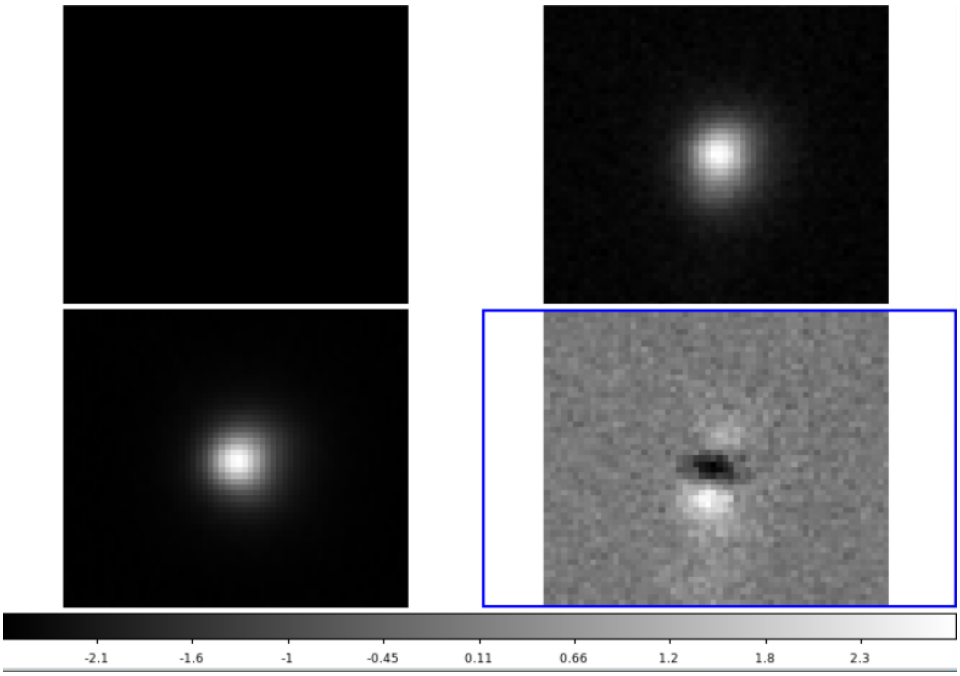

Figure 1.13.: The image block generated by galfit assuming there is only *one* image. First image is intended to be empty. Second and third are respectively original and modelled images. Last one shows the residuals.

1.7. Time-delay estimate

Time delay between two images can be estimated using minimal dispersion method. But a large number of observations are needed for it to work. Thus we take the data of [6] and the raw data are presented in appendix A.4.

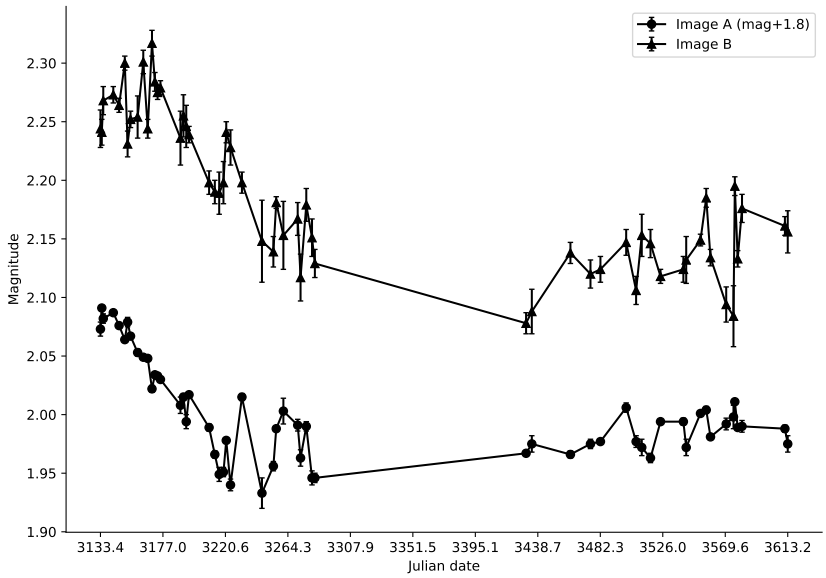

Figure 1.14.: Light curves of two images. Note that image A is originally much dimmer. For better comparison, its magnitude is added with 1.8.

Before using minimal dispersion method, one can try to inspect the light curves visually. Figure. 1.14 shows the light curves. Most noticeable feature is a large gap between observations caused by limited observation window. Time delay is quite hard to discern in this plot, but if there is it should be $\mathcal{O}(10)$ days. There is also quite a magnitude difference.

To reliably determine time delay of two images, one has to use minimal dispersion method, implemented in program `tdel`. Before one turns Monte Carlo function on, one should roughly find good input parameters of the program, so that the true global minimum can be found. Parameters are listed in table. A.2.

Time delay is determined to be

$$\lambda = 34.29 \text{ days} \tag{1.37}$$

Dispersion spectra of this preliminary run are figure 1.15a, 1.15b, and 1.15c. Note the magnitude shift here refers to the magnitude shift after an initial adjustment, so that in the end minimal dispersion should be located at somewhere near zero magnitude shift. Indeed, the dispersion spectra show no clear minima within the selected region, except for zero magnitude shift. So we are certain that we found a global minimum.

Also from part 1.3, we know that near the minimum dispersion can be approximated by a parabola. One can quantify the goodness of fitting of data points in figure 1.15a, 1.15b, and 1.15c using χ^2. χ^2 has a clear minimum at zero "time delay", shown in figure 1.16

With this knowledge and input parameters, Monte Carlo is turned on and it gives us

$$\lambda = 34.336 \pm 2.184 \text{ days} \tag{1.38}$$

Here Monte Carlo method also gives us probabilities of various time delays, see figure. 1.17. Fitting using function

$$f(t) = \frac{1}{\sigma\sqrt{2\pi}} \exp\left(-\frac{1}{2}\frac{(t-\mu)^2}{\sigma^2}\right)$$

determined the parameters and covariance matrix to be

$$\begin{aligned}
\mu &= 33.959 \\
\sigma &= 1.988 \\
\Sigma &= \begin{pmatrix} 0.0064 & -0.0002 \\ -0.0002 & 0.004 \end{pmatrix}
\end{aligned}$$

Note that here the fit function does not have either multiplicative or additive constant, since we have probability directly. These values are very close to direct output of Monte Carlo. So one may say the result of Monte Carlo is realistic.

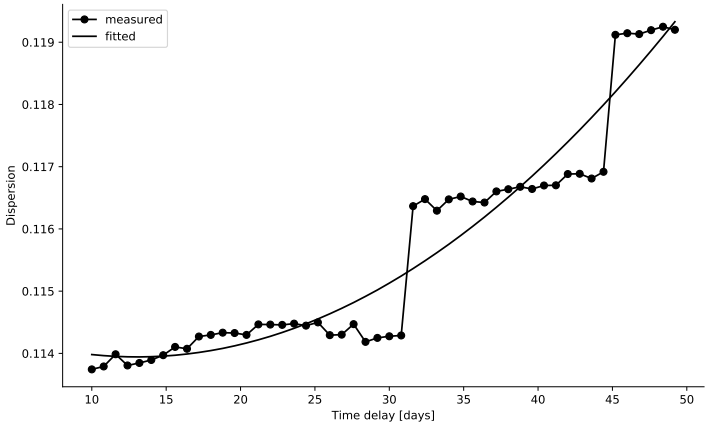

(a) magnitude shift=−2.5

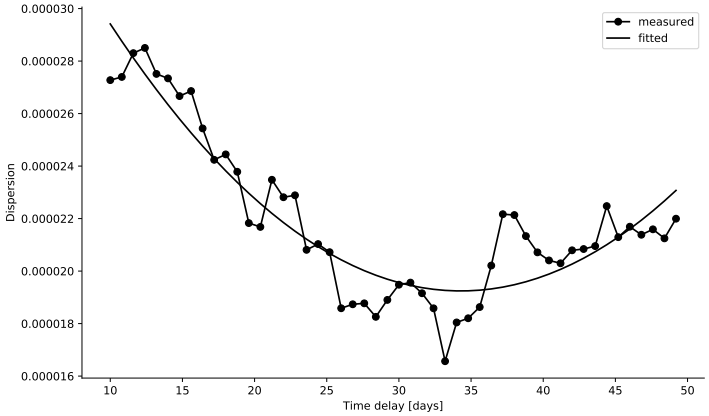

(b) magnitude shift=0

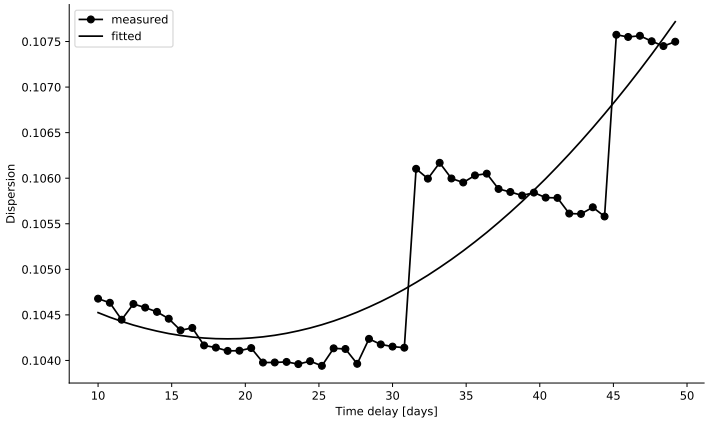

(c) magnitude shift=2.4

Figure 1.15.: Dispersion spectra with various magnitude shifts.

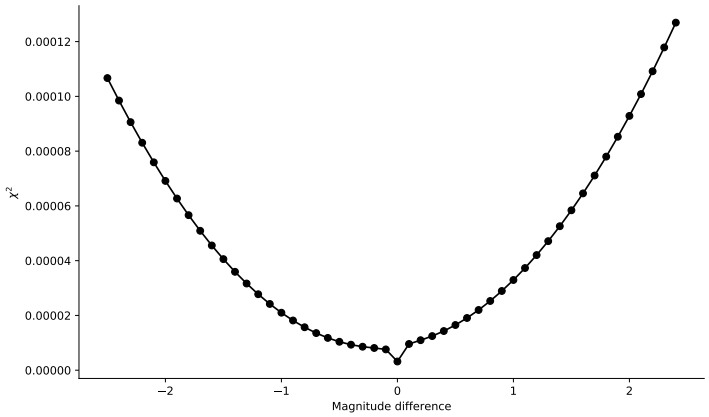

Figure 1.16.: Goodness of fit. Smaller the better.

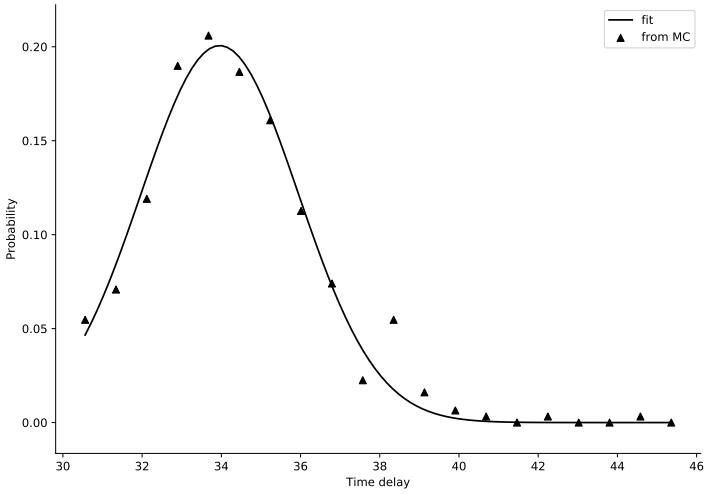

Figure 1.17.: Probability of different time delays estimated by Monte Carlo method. Raw data in appendix. A.6

1.8. Lensing analysis

Calculation with accepted value of H_0 Since the redshifts of lens and source system are known, one can from image separation determine the velocity dispersion in SIS model. Angular distances should be computed also by equation. 1.6. Here the cosmological parameters are taken from [7]

$$\Omega_m = 0.3089 \pm 0.0062, \quad \Omega_\Lambda = 0.6911 \pm 0.0062$$

For simplicity, errors in these parameters are not propagated in further analysis (almost negligible). For this part, currently accepted value of H_0 is used.

Image separation can be used to compute Einstein radius. Results of `galfit` are in pixels, so they need to be converted to angles first. As given in [3], one pixel corresponds to $0.177''$. Image separation can be expressed by Einstein radius with equation. 1.30. The separation in pixels and in radians are then

$$\begin{aligned}
\Delta r &= 6.600 \pm 0.079\,(\text{pixels}) \\
\Delta\theta &= 1''.170 \pm 0''.014 = (5.667 \pm 0.068) \cdot 10^{-6} \\
\theta_E &= (2.834 \pm 0.034) \cdot 10^{-6}
\end{aligned}$$

Here the error is properly propagated using

$$\begin{aligned}
\sigma_{\Delta r}^2 &= \left(\frac{\partial \Delta r}{\partial x_A}\right)^2 \sigma_{x_A}^2 + \left(\frac{\partial \Delta r}{\partial y_A}\right)^2 \sigma_{y_A}^2 + \left(\frac{\partial \Delta r}{\partial x_B}\right)^2 \sigma_{x_B}^2 + \left(\frac{\partial \Delta r}{\partial y_B}\right)^2 \sigma_{y_B}^2 \\
&= \frac{1}{(\Delta r)^2}\left[(x_A - x_B)^2(\sigma_{x_A}^2 + \sigma_{x_B}^2) + (y_A - y_B)^2(\sigma_{y_A}^2 + \sigma_{y_B}^2)\right]
\end{aligned}$$

With equation. 1.20, one finds

$$\sigma_v = (6.594 \pm 0.040) \cdot 10^{-4} c \tag{1.39}$$

where the error is given by

$$\sigma_{\sigma_v} = \frac{\sigma_v}{2\theta_E}\sigma_{\theta_E}$$

According to equation. 1.19, projected mass inside Einstein radius is computed to be

$$M(\theta < \theta_E) = (2.246 \pm 0.054) \cdot 10^{41}\text{kg} = (1.129 \pm 0.027) \cdot 10^{11} M_\odot \tag{1.40}$$

This has similar magnitude as the estimated mass of milky way ($\sim 1 \times 10^{12} M_\odot$) [8]. The error is propagated to be

$$\sigma_M = \frac{2M}{\theta_E}\sigma_{\theta_E}$$

Determination of H_0 By looking at equation (1.33), it is certain that we need not only the separation but also the position of two images in order to compute H_0. This information can be extracted using the flux ratio or magnitude difference

$$\Delta m = m_1 - m_2 = \underbrace{-(100^{1/5})}_{=:1/A} \log_{10}\left(\frac{S_1}{S_2}\right) \tag{1.41}$$

By inverting this and from equation (1.36), we have

$$\frac{S_A}{S_B} = 0.210 = \frac{\theta_A}{\theta_B} \tag{1.42}$$

Error is calculated by

$$\sigma_{S_A/S_B} = A\ln(10)\sqrt{10^{2Am_A}\sigma_{m_A}^2 + 10^{-2Am_B}\sigma_{m_B}^2} \approx 4 \times 10^{-10}$$

This error is too small and will be neglected in further analysis.

Image separation is also known, thus the image angular positions relative to the lens system can be calculated

$$\begin{aligned} \theta_A &= -(1.51 \pm 0.02) \cdot 10^{-6} \\ \theta_B &= -(7.18 \pm 0.09) \cdot 10^{-5} \end{aligned} \tag{1.43}$$

Now we have all the ingredients in (1.33) to determine Hubble constant. Introduce the dimensionless angular distance

$$D'(z_1, z_2) = \frac{H_0}{c} D(z_1, z_2)$$

Then we have

$$H_0 = \frac{1}{2\Delta t}(1 + z_d)\frac{D'_d D'_s}{D'_{ds}}(\theta_A^2 - \theta_B^2) \tag{1.44}$$

The sign of H_0 must be positive. We are not certain how to properly pair the images of `galfit` and time delay analysis. So in the end, we just add minus sign to make Hubble constant positive. We have

$$H_0 = (246.47 \pm 15.68)\,\mathrm{km\,s^{-1}\,Mpc^{-1}} \tag{1.45}$$

1.9. Conclusion

In this chapter, we analyzed one pair of lens images, most importantly image separation and magnitude ratio are extracted. Combined with another independent observation, we determine the Hubble constant.

Just from the numerical value of the determined H_0, it is quite questionable already. Comparing to some other reputable measurements [9][10] for example, this value is roughly off by a factor of three. The origin of this discrepancy should be the lens model. SIS model is an axial symmetric model, where the sketch in [3] objects are not properly aligned. The result we obtained is not realistic.

In [11], they have basically the same data: image separation $1''.2$, and $\sim 1:5$ flux ratio in R-band. However, because of the clear asymmetry, SIS model with a shear term is used. In the end, they are able to predict ~ 33 days time delay using the reasonable Hubble constant $H_0 = 75\,\mathrm{km\,s^{-1}\,Mpc^{-1}}$. So the inaccurate lens model should be blamed for this awful determination of H_0.

2. Bad weather

2.1. Introduction

In this part of this experiment, we determine the properties of CCD mounted at the telescope. Some parts are of great importance for the lensing part, since it directly tells us the quality of images we take.

These measurements have already carried out prior to the actual lab session. In this lab, we can measure the dark current and its dependence on temperature, the detector gain, read-out noise, linearity, and full well capacity.

2.2. Background

2.2.1. Observations in Optical Astronomy

Telescope Optics

In our observation we used a 50 cm reflector telescope of the Cassagrain type which is available in AIFA. A schematic diagram of this telescope is as shown in Fig. 2.1.

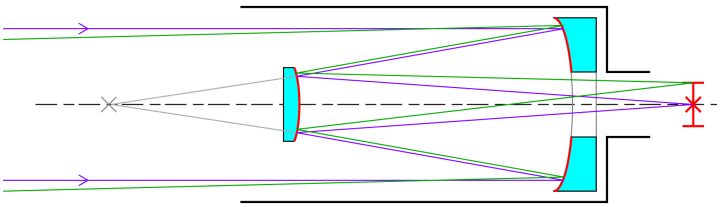

Figure 2.1.: Schematic light path in a Cassegrain telescope[3].

Magnitude

In optical astronomy, the optical brightness of a source is called magnitude.

The difference in magnitudes between two sources is defined on the basis of ratio of their observed fluxes S_1 and S_2 as,

$$\Delta m = m_1 - m_2 = -(100^{1/5}).\log_{10}\left(\frac{S_1}{S_2}\right) \tag{2.1}$$

With this definition, fainter sources have higher magnitude.

Coordinate system

There are different co-ordinate systems use to quantify the position of celestial objects in optical astronomy. The equatorial system is a most common system for identifying and cataloging the

sources. In this system the framework of terrestrial latitude and longitude projected from the centre of earth onto the sky [3].

- Declaration is an analogy to latitude in geography. Here, the north pole having declination of $\delta = 90°$ and projection of south pole is $\delta = -90°$. It is express as degree, minute and second.
- Right Ascension, α, is equivalent to longitude with the equatorial zero point. It is express as hour, minute and second.

2.2.2. Charge-coupled device

Charge-coupled devices (CCD) are two-dimensional detector used to detect electromagnetic radiations. It response wide wavelength range (from near infrared to the soft X-ray). Its working principle relies on photoelectric effects, thus usually highly linear [3].

Good quality CCDs have high quantum efficiency, low read noise, and excellent linearity. In this experiment we will determine these properties. Some of these properties are discussed below.

Stability

There are several aspect to hold excellent stability characteristic by a CCD. Some of them are

- CCD is geometrically very stable because it is contracted by pure silicon.
- It keeps its performance over years without degradation.
- It has very high sensitivity; however, very insensitive to over-exposure.

Dark Current

The dark current is a thermal noise. It depends on the temperature of CCD. At room temperature, it fills CCD pixels to their saturation level within a short period of time (a minute or even less). Therefore, it is necessary to keeps the detector system at a low temperature. The cooing of CCD is done thermo-electrically with closed cycle system or by using liquid nitrogen [3].

The dark current, I_{dark} changes with temperature, T, as

$$I_{\text{dark}} = cT^{3/2} e^{-\frac{E_g}{2k_{\text{B}}T}} \tag{2.2}$$

where $E_g = 1.16\,\text{eV}$ is the silicon band gap energy, $k_{\text{B}} = 8.62 \times 10^{-5}\,\text{eV}\,\text{K}^{-1}$ is the Boltzmann constant, and c is a detector specific constant. In this report, dark current is always given in unit of $\text{e}\,\text{p}^{-1}\,\text{s}^{-1}$, i.e. before A/D conversion.

Gain

The ratio between the amount of charge in a CCD pixel and the corresponding digital number after A/D conversion is called detector gain k [3]. It is measured in the unit of e^-/ADU. It can be calculation on the basis of the assumption that photon detector is Poisson distributed [3].

$$N_e = \sigma_e^2 = kN_{e,d} = k^2\sigma_{e,d}^2 \tag{2.3}$$

where N_e and σ_e are average number of electron and its variance. Subscript d means that the numbers are converted to ADU already. Therefore, the gain can be determined with

$$k = \frac{N_{e,d}}{\sigma^2_{e,d}} \tag{2.4}$$

Quantum Efficiency

Quantum efficiency is defined as the ratio of produced electrons to the number of photons hitting the detector surface [3]. Top order CCDs have the significant wavelength range more than 90%.

Read-Out Noise

Even fully covered CCD still have signals varying from pixel to pixel due to the amplification noise occurring in the electronics. The standard deviation of this scatter is called read out noise [3].

Noise

Noise always means that the standard deviation of the signal level. In our detector system there are three sources of noise: read-out noise, photon noise and PRNU noise. The so-called Pixel Response Non-Uniformity (PRNU) noise is pixel to pixel variation caused by difference quantum efficiency. Thus the total noise is given by [3]

$$\sigma_{\text{tot}} = \sqrt{\sigma^2_{\text{RON}} + \sigma^2_e + \sigma^2_{\text{PRNU}}} \tag{2.5}$$

where σ_{PRNU} is proportional to signal level,

$$\sigma_{\text{PRNU}} = N_e f_{\text{PRNU}} \tag{2.6}$$

f_{PRNU} is a detector dependent characteristic PRNU factor. It is typically in the order of 0.01 [3].

Linearity and full-well capacity

One the most appealing feature of CCDs as astronomical detectors is their linearity. Here, the output signal is proportional to the incoming photons received by the detector. They are linear over the full dynamic range of 10^4 to 10^5 and deviation from linearity is just $\pm 0.5\%$ for well behaved system [3].

The CCD pixels have limited charge capacity. The maximal number of the electrons fitting into a single pixel is called full-well capacity. If one pixel site gets full, electrons will start to spill over to adjacent pixels, causing the so-called blooming effect [3]. Saturation level is essentially the same thing as full-well capacity, but given in the unit of ADU.

2.3. Dark current

All data used in this chapter are already taken beforehand and provided to us. Three images with 30 s, 60 s, and 120 s exposure times are taken at temperature between −10 °C and 10 °C with step of 2 °C. Raw data can be found in appendix A.7.

Data with `imstats` are taken in region $1800 < x < 2800, 300 < y < 800$. Mean of the images is chosen as the measure of dark current and bias. It might be influences by cosmic rays, random fluctuations and so on. But it also has variance (sigma) provided. Variance can be used further in curve fitting process. In the end, mode, mean and median don't differ from each other very much, if one looks at the raw data anyway.

For every temperature, a linear fitting is done to the three data points. Slope corresponds to dark current *after* converted by gain. Intercept can be interpreted as bias level. These two quantities are plotted in figure 2.2, 2.3.

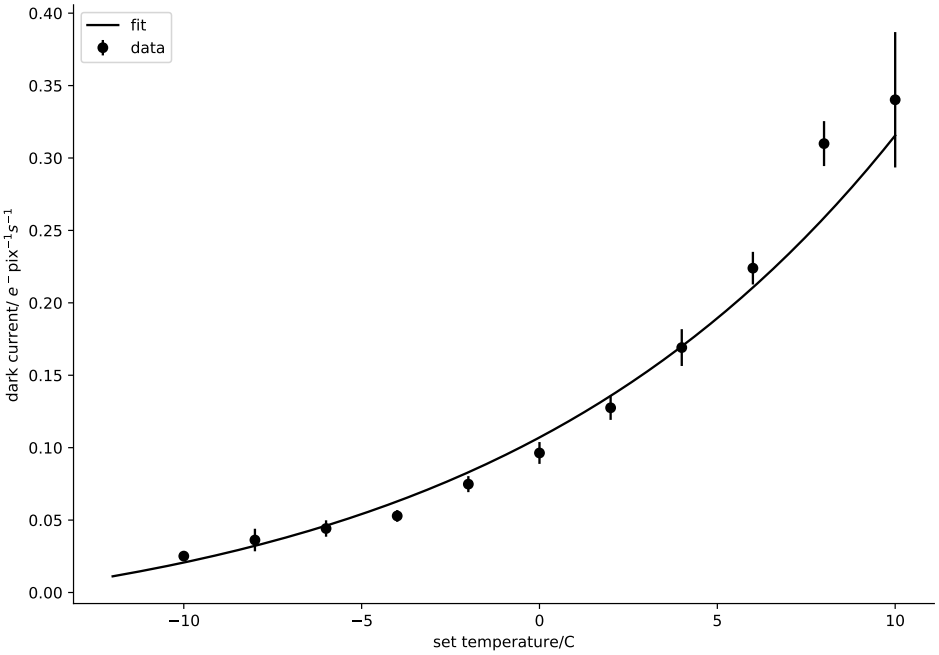

Figure 2.2.: Dark current. Obtained from slope of points at one temperature and then converted to in unit of e^-.

Since slope and intercept are calculated from the same fitting process, there are correlation between these two to some extent. For simplicity, correlations are ignored and only the diagonal entries of the covariance matrix are used in further discussion. Errors drawn in figure 2.2 and 2.3 are thus the diagonal part of the matrix. Dark current is here given in unit of $\mathrm{e\,p^{-1}\,s^{-1}}$, thus we want to convert it using gain from later parts (section 2.4 and 2.5). These two values are combined (averaged) and their errors are propagated properly (variance is additive). The gain used here is

$$k = (1.49 \pm 0.05)\,\mathrm{e\,ADU^{-1}}$$

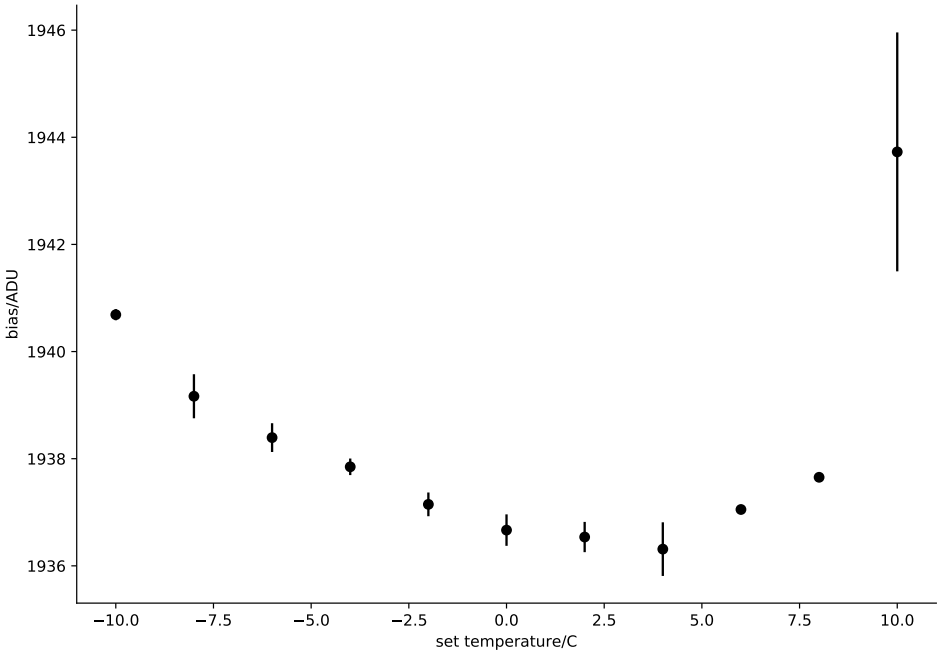

Figure 2.3.: Bias from intercept of linear fitting

Error of dark current is given in

$$\sigma_{I_{\mathrm{dark}}} = I_{\mathrm{dark}} \sqrt{\left(\frac{\sigma_k}{k}\right)^2 + \left(\frac{\sigma_{I_{\mathrm{dark,d}}}}{I_{\mathrm{dark,d}}}\right)^2}$$

In figure 2.3, bias levels somewhat depend on the temperature as well. This might be understood because the determined dark current and bias have correlation in the fitting process. Or maybe the cooling also affects the read-out circuit. Anyway this fluctuation is really tiny ($\sim 0.2\%$).

The fit curve in figure 2.2 is done with equation 2.2, but with extra additive constant A. This constant makes the fitting so much better. The origin of this constant is still puzzle to us. With it, dark current at quite low temperature could be negative, thus the model breaks down. These parameters are

$$c = (1\,516\,853.877 \pm 90\,255.383)\,\mathrm{e\,p^{-1}\,s^{-1}\,K^{-3/2}}$$
$$A = (-0.030 \pm 0.005)\,\mathrm{e\,p^{-1}\,s^{-1}}$$

Expected dark current at $T = -25\,^{\circ}\mathrm{C}$ would be

$$I_{\mathrm{dark}}(T = -25\,^{\circ}\mathrm{C}) = (-0.030 \pm 1.035)\,\mathrm{e\,p^{-1}\,s^{-1}}$$

This amount of dark current would not affect image quality in HOLIGRAIL observations too much. An exemplar science frame has exposure time of 300 s and then noise due to dark current would be about 6 ADU. This is negligible since the "background" of the science has typically ~ 600 ADU and bias has something like ~ 200 ADU.

In figure 2.3 and 2.2, one might see the x-axis is the set temperature instead of real temperature. Quite understandable there are some fluctuations around the set temperature, since

the temperature control circuit/chip cannot be perfect. These fluctuations are not taken in consideration while doing the (first set of) curve fits to find dark current. By doing this the errors are not underestimated, since these fluctuations would also influence the pixel values at different exposure times. It will leads to (usually) larger uncertainties in dark current and bias. One could try to use model function with the determined parameters to correct the temperatures to the set values. But it would not be necessary and potentially problematic, because the data might have some bias towards the existing parameters.

2.4. Detector system "gain" and noise

For this part, one bias and two flats are provided. In order to get rid of the PRNU noise, a difference frame of these two flats is generated with the command `ic` provided in [3].

Bias frame contains only the RON, since it is not exposed to light. Difference frame only have RON and photon noise

$$\sigma^2_{\text{diff, d}} = 2\sigma^2_{\text{RON, d}} + 2\sigma^2_{e,\text{d}}$$

The factor 2 arises because the variance is additive when calculating difference of two images. Then one can subtract the RON from bias frame to extract the photon noise

$$\sigma_{e,\text{d}} = 144.81\,\text{ADU} \tag{2.7}$$

In principle, PRNU noise can be extracted in the same way, whereas we have here two flat images. Thus signal levels of two images get averaged (one can obtain an error estimate by the way) and their variance as well according to propagation of uncertainties

$$N_{e,\text{d}} = (31\,742.94 \pm 7.85)\,\text{ADU}$$
$$\sigma_{\text{flats, d}} = \frac{1}{2}\sqrt{\sigma^2_{\text{flat, d,1}} + \sigma^2_{\text{flat, d,2}}}$$

Subtracting two previous computed noises, we have the PRNU noise

$$\sigma_{\text{PRNU, d}} = 140.38\,\text{ADU} \tag{2.8}$$

With equation 2.6,

$$f_{\text{PRNU}} = (4.422 \pm 0.001) \cdot 10^{-3} \tag{2.9}$$

This has similar order of magnitude as given in [3].

One could determine the gain with the help of equation 2.4. It is

$$k = (1.514 \pm 0.000)\,\text{e}\,\text{ADU}^{-1} \tag{2.10}$$

As a reference, the RON noise in unit of electron is

$$\sigma_{\text{RON}} = (14.881 \pm 0.004)\,\text{e} \tag{2.11}$$

2.5. Detector linearity and full-well capacity

Again, the data are already taken and we assume that these images are ordered randomly to avoid systematic effects. These images are taken with red filter and the set temperature

is $-10\,°\mathrm{C}$. The signal level and other informations are evaluated in a uniformly illuminated region: $1200 < x < 1600$ and $400 < y < 600$. Raw data can be found in appendix A.10.

Once pixels in CCD get saturated, pixel count increase non-linearly. This can be easily seen in signal level against exposure time plot, see figure 2.4. Signal level refers to the mean pixel counts in the image. Here the fitting is done only to the points roughly on a straight line. This line is described by

$$S(t) = a \cdot t + b = 61\,097.242\,\mathrm{ADU\,s^{-1}} \cdot t + 2091.783 \tag{2.12}$$

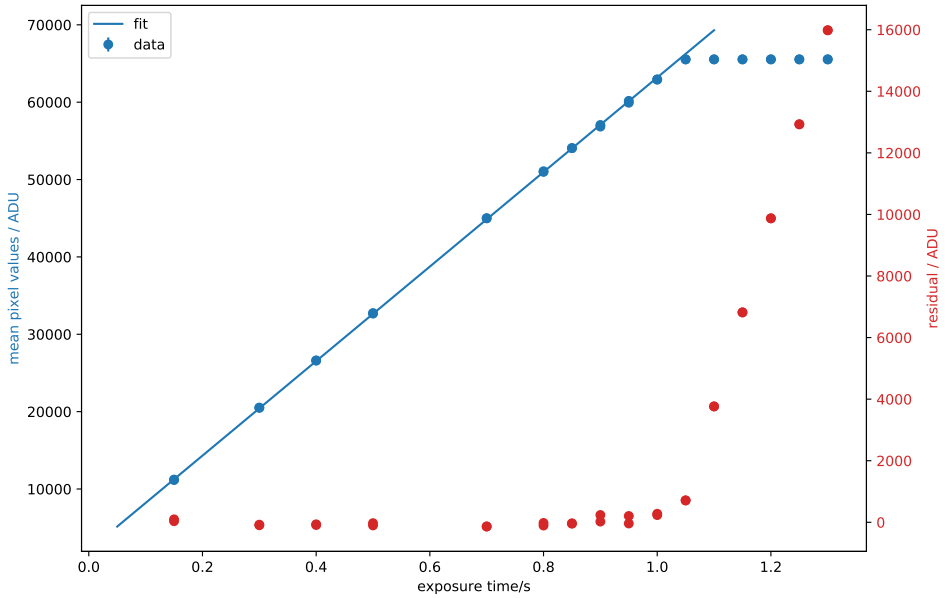

Figure 2.4.: Signal level (mean) against exposure time and residuals.

Using this expression we can calculated exposure time given some signal levels. Covariance matrix (of the fit parameters) is

$$\Sigma_{ab} = \begin{pmatrix} 6917.573 & -2829.764 \\ -2829.764 & 1702.991 \end{pmatrix}$$

Clearly this matrix is not (loosely) diagonal, thus the parameters are somewhat correlated. Inverting the function in equation 2.12 gives us a non-linear function in parameters a and b. Nonetheless, one could just the mighty Taylor expansion and use the Jacobian to try to propagate the errors

$$\Sigma_t = J \Sigma_{ab} J^T \tag{2.13}$$

Maximal exposure time without saturation can be computed using 2.12, its error using 2.13. Non-linearity kicks in at exposure time of $1.034\,\mathrm{s}$. The error is really tiny at $8.8 \cdot 10^{-7}\mathrm{s}$.

In fact, this determination can be improved by looking into difference frames of images with identical exposure time. Two frames with identical exposure time are recorded and get subtracted. The variance (or sigma) in difference frame will drop significantly, as soon as CCD gets saturated. So in principle, one can determine the maximal exposure time without saturation more precisely.

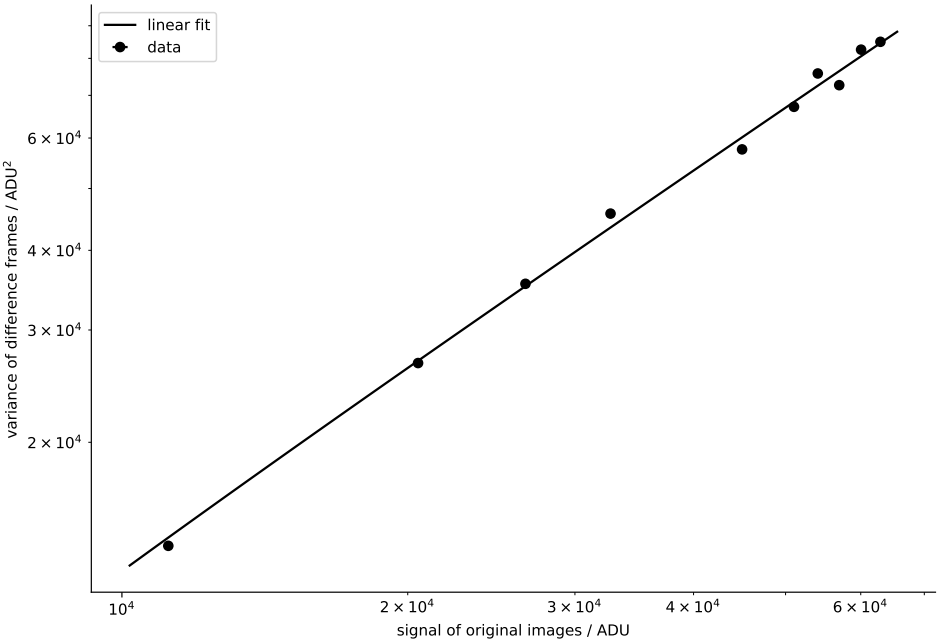

Figure 2.5.: Sigma against signal levels in log-log scale. At large exposure time, CCD gets fully saturated, thus the sigma is zero and corresponding data points cannot show up in log scale. Errors of signal level are taken as the sigma of the respective image, but not visible here.

In figure 2.5, this drop is not so obvious, since after the steady climb the variance of difference frame goes to zero immediately. We claim that after the last point in figure 2.5 is where CCD gets saturated. Just as a rough estimate, saturation level is calculates as the mean value of the last point shown in figure 2.5 and its next point (with zero variance) and error is taken as the distance to each of these two points: $(64\,233.35 \pm 2599.89)\,\mathrm{ADU}$.

The straight line (at least in normal scale) is parameterized as

$$\sigma^2(N) = a \cdot N + b = 1.36\,\mathrm{ADU} \cdot N + (-1038.89\,\mathrm{ADU}^2)$$

with covariance matrix

$$\sigma_{ab} = \begin{pmatrix} 1.78 \times 10^{-3} & 75.13 \\ -75.13 & 3.69 \times 10^{6} \end{pmatrix} \tag{2.14}$$

The slope can be used to compute the gain k using equation 2.4. Unfortunately, real life is complicated as always. The pixel value of the difference frame is a linear combination of individual frames (difference). Thus the variance simply add with each other. Here the fixed pattern noise is irrelevant, since it doesn't vary between exposures. Thus the pixel value of difference frame will only contain statistical error (photon noise). We have now

$$k = \frac{N_{e,d}}{\sigma^2_{\mathrm{diff}}/2} \tag{2.15}$$

Thus the slope of the line is $\frac{2}{k}$. Assuming that the fit parameters are uncorrelated and we just take the diagonal entries as the uncertainty for the slope. The gain is determined to be

$$k = (1.47 \pm 0.05) e^- \mathrm{ADU}^{-1} \tag{2.16}$$

Its error is propagated with

$$\sigma_k = \left| \frac{2}{a^2} \sigma_a \right|$$

With the value of gain, saturation value can be converted to in units of e^-, i.e. full-well capacity

$$\text{full-well} = (94\,479.66 \pm 4820.67) e^- \tag{2.17}$$

where the error is computed by

$$\sigma_{\text{fw}}^2 = \text{fw} \cdot \sqrt{(\sigma_k/k)^2 + (\sigma_{\text{sat}}/\text{sat})^2}$$

2.6. Conclusion

We have successfully determined several properties of the CCD chip. Dark current and its dependence on temperature. With the obtained information, we can extrapolate to compute dark current at $-25\,°\text{C}$ and find it will not affect HOLIGRAIL observations. Detector gain is calculated by two different methods and they deliver consistent results. Full-well capacity (saturation level) is determined to relatively high precision.

One can try to compare data from analysis and their reference values. The model name of the CCD chip can be found in the header file: `SBIG STL-6303 3 CCD Camera`. It seems to be commercially available and its specifications are listed for example [12]

- gain: 1.4 unbinned
- full-well capacity: $100\,000 e^-$

Images we have should all be unbinned, since the header shows the binning is 1×1. Full-well capacity lies roughly 1σ away from the literature value.

A. Appendix

A.1. LIST file

COL	LINE	RMAG	FLUX	SKY	PIXELS	R	ELLIP	PA	PEAK	MFWHM
293.05	1859.53	19.30	191.3	0.15	80	3.51	0.019	82.5	3.98	7.96
435.95	1647.42	18.24	505.1	0.40	79	3.50	0.011	−63.1	10.49	8.12
974.61	1522.59	16.49	2531.7	2.10	79	INDEF	0.029	−38.3	52.22	8.16
652.00	1365.48	19.99	101.2	0.09	78	2.88	0.056	83.9	2.14	7.93
851.99	603.17	18.72	326.0	0.27	77	1.64	0.022	72.2	6.86	8.20
623.70	265.30	19.54	153.1	0.11	81	4.12	0.022	−13.9	3.18	7.88
279.06	1492.48	18.34	459.4	0.36	80	3.11	0.022	81.2	9.48	8.03
549.09	975.02	19.86	113.3	0.12	75	INDEF	0.015	68.6	2.32	8.71

A.2. galfit.input

```
# IMAGE and GALFIT CONTROL PARAMETERS
A) new_cutscale8.fits                    # Input data image (FITS file)
B) new2_cutscale8.fits                   # Output data image block (FITS file)
C) none                # Sigma image name (made from data if blank or "none")
D) cut_star_stack_scale.fits                    # Input PSF image (FITS file)
E) 1                   # PSF fine sampling factor relative to data
F) none                # Bad pixel mask (FITS image or ASCII coord list)
G) none                # File with parameter constraints (ASCII file)
H) 0   60   0   60  # Image region to fit (xmin xmax ymin ymax)
I) 100     100         # Size of the convolution box (x y)
J) 26.0                # Magnitude photometric zeropoint
K) 0.038   0.038       # Plate scale (dx dy)   [arcsec per pixel]
O) both                # Display type (regular, curses, both)
P) 0                   # Options: 0=normal run; 1,2=make model/imgblock & quit
S) 1                   # Modify/create objects interactively?



# INITIAL FITTING PARAMETERS
#
# column 1: Parameter number
# column 2: initial gues for value
# column 3: allow parameter to vary (yes = 1, no = 0)
# column 4: comment



# Component 1:
# PSF fit.

 0) psf                # object type
 1) 30   31    1 1     # position x, y    [pixel]
 3) 16          1      # total magnitude (only relative values are relevant)
 8) 1           0      # axis ratio (<=1)
 Z) 0                  # leave in [1] or subtract [0] this comp from data?



# Component 2:
# PSF fit.

 0) psf                # object type
```

```
 1) 31   31    1 1      # position x, y    [pixel]
 3) 18          1       # total magnitude (only relative values are relevant)
 8) 1           0       # axis ratio (<=1)
 Z) 0                   # leave in [1] or subtract [0] this comp from data?


# Component 3:
# sky background

 0) sky                 # object type
 1) 1.71          1     # sky background    [ADU counts]
 2) 0.000         0     # dsky/dx (sky gradient in x)
 3) 0.000         0     # dsky/dy (sky gradient in y)
 Z) 0                   # leave in [1] or subtract [0] this comp from data?
```

A.3. Output of galfit

First group of output is the fitting of two components (images), second group with only one component. Coordinates shown in curly brackets are the coordinates and their errors according to [5]. In our analysis, the variables/errors are interpreted as uncorrelated, so that a simple propagation of error formula can be used.

```
Input image      : new_cutscale8.fits[1:60,1:60]
Init. par. file  : galfit.input
Restart file     : galfit.02
Output image     : new2_cutscale8.fits

 psf       : (29.69, 24.71)    19.20
               (0.05, 0.08)    0.02
 psf       : (31.11, 31.16)    17.50
               (0.01, 0.01)    0.00
 sky       : [30.50, 30.50]    1.72      0.00e+00    0.00e+00
                               0.00      0.00e+00    0.00e+00
 Chi^2 = 160040.84238,   ndof = 3593
 Chi^2/nu = 44.542
```

```
Input image      : new_cutscale8.fits[1:60,1:60]
Init. par. file  : galfit_onesource.input
Restart file     : galfit.03
Output image     : newOne_cutscale8.fits

 psf       : (30.93, 30.48)    17.37
               (0.01, 0.01)    0.00
 sky       : [30.50, 30.50]    1.76      0.00e+00    0.00e+00
                               0.01      0.00e+00    0.00e+00
 Chi^2 = 365406.61697,   ndof = 3596
 Chi^2/nu = 101.615
```

A.4. Raw data of time delay estimate

HJD	seeing [″]	mag A	σ_A	mag B	σ_B	mag star #5	$\sigma_{star\#5}$
3 133.412	1.5	0.273	0.006	2.244	0.016	−0.175	0.013
3 134.362	1.1	0.291	0.002	2.241	0.011	−0.166	0.004
3 135.385	0.9	0.282	0.004	2.268	0.012	−0.177	0.008
3 142.386	1.3	0.287	0.002	2.273	0.007	−0.167	0.003
3 146.415	1.2	0.276	0.001	2.264	0.006	−0.178	0.002
3 150.406	0.9	0.264	0.001	2.300	0.006	−0.176	0.001
3 152.367	1.0	0.279	0.004	2.231	0.011	−0.172	0.008
3 154.407	0.9	0.267	0.002	2.252	0.007	−0.175	0.003
3 159.364	1.1	0.253	0.003	2.254	0.018	−0.174	0.005
3 163.315	1.7	0.249	0.002	2.301	0.010	−0.173	0.003
3 166.425	1.0	0.248	0.002	2.244	0.008	−0.177	0.003
3 169.393	1.1	0.222	0.003	2.317	0.011	−0.189	0.006
3 171.430	1.5	0.234	0.002	2.284	0.008	−0.172	0.004
3 173.298	1.1	0.233	0.001	2.275	0.006	−0.168	0.002
3 175.300	1.1	0.230	0.001	2.279	0.006	−0.178	0.001
3 189.265	1.1	0.208	0.007	2.236	0.023	−0.172	0.012
3 191.360	1.1	0.215	0.003	2.255	0.018	−0.167	0.004
3 193.304	1.3	0.194	0.006	2.246	0.018	−0.166	0.012
3 195.252	1.0	0.217	0.002	2.239	0.007	−0.170	0.004
3 203.314*	1.4	0.186	0.001	2.345	0.007	−0.173	0.002
3 209.256	1.0	0.189	0.003	2.198	0.010	−0.167	0.007
3 213.256	1.0	0.166	0.003	2.190	0.010	−0.183	0.007
3 216.310	1.7	0.149	0.006	2.189	0.018	−0.163	0.011
3 219.281	1.6	0.151	0.004	2.198	0.018	−0.155	0.008
3 221.234	1.0	0.178	0.002	2.241	0.009	−0.179	0.003
3 224.209	1.2	0.140	0.005	2.228	0.015	−0.166	0.010
3 232.187	1.1	0.215	0.003	2.198	0.009	−0.168	0.005
3 246.163	1.3	0.133	0.013	2.148	0.035	−0.142	0.026
3 248.138*	1.5	0.172	0.004	2.054	0.013	−0.114	0.007
3 254.125	0.9	0.156	0.004	2.139	0.013	−0.160	0.007
3 256.135	1.0	0.188	0.001	2.181	0.005	−0.173	0.003
3 261.115	1.5	0.203	0.011	2.153	0.029	−0.178	0.017
3 271.109	1.3	0.191	0.005	2.167	0.014	−0.183	0.009
3 273.103	1.2	0.163	0.007	2.117	0.020	−0.176	0.013
3 277.104	1.0	0.190	0.004	2.179	0.014	−0.191	0.007
3 281.106	1.4	0.146	0.006	2.151	0.016	−0.167	0.011
3 283.100	1.2	0.146	0.004	2.129	0.012	−0.164	0.008
3 430.540	0.9	0.167	0.002	2.078	0.009	−0.135	0.003
3 434.546	0.8	0.175	0.007	2.088	0.019	−0.143	0.009
3 461.499	0.9	0.166	0.003	2.138	0.009	−0.150	0.005

Table A.1.: Photometry of SDSS1650 and of reference star #5, as in Fig. 1.14. The Julian date corresponds to HJD-2 450 000 days. The five points marked by an asterisk are not used in the determination of the time delay.

HJD	seeing [″]	mag A	σ_A	mag B	σ_B	mag star #5	$\sigma_{star\#5}$
3 475.491	0.9	0.175	0.004	2.120	0.012	−0.179	0.008
3 482.443	1.1	0.177	0.002	2.124	0.011	−0.149	0.004
3 500.415	1.3	0.206	0.004	2.147	0.011	−0.168	0.008
3 507.348	1.0	0.177	0.005	2.106	0.012	−0.153	0.009
3 508.403*	0.9	0.199	0.003	2.222	0.009	−0.171	0.006
3 511.303	1.0	0.172	0.007	2.153	0.018	−0.151	0.012
3 517.383	0.8	0.163	0.004	2.146	0.012	−0.168	0.007
3 524.391	0.9	0.194	0.002	2.118	0.006	−0.183	0.003
3 533.412*	1.6	0.193	0.002	2.002	0.007	−0.171	0.004
3 540.345	1.0	0.194	0.003	2.124	0.011	−0.168	0.006
3 542.323	1.1	0.172	0.007	2.132	0.020	−0.194	0.014
3 552.291	0.9	0.201	0.001	2.149	0.005	−0.179	0.001
3 556.295	0.9	0.204	0.003	2.185	0.008	−0.176	0.005
3 559.280	1.0	0.181	0.002	2.134	0.007	−0.160	0.004
3 564.295*	1.3	0.228	0.001	2.300	0.007	−0.167	0.003
3 570.247	1.0	0.192	0.005	2.094	0.015	−0.165	0.010
3 575.323	1.3	0.198	0.010	2.084	0.026	−0.172	0.019
3 576.264	1.0	0.211	0.001	2.195	0.008	−0.181	0.002
3 578.275	1.2	0.189	0.002	2.133	0.007	−0.177	0.003
3 581.284	1.2	0.190	0.005	2.176	0.012	−0.188	0.009
3 611.225	1.2	0.188	0.003	2.161	0.008	−0.165	0.005
3 613.201	1.5	0.175	0.007	2.156	0.018	−0.180	0.013

A.5. Input parameters of program tdel

parameter	value
Delay_guess	30
Delay_Min	10
Delay_Max	50
Delay_nbin	10
mmag_Max	-2.5
mmag_Min	2.5
mmag_nbin	50
UseMC	0
NMC	0
MinGapLength	100

Table A.2.: Initial content of tdel.param. Some other inputs are not shown here, since they remain unchanged from default values. Later Monte Carlo is turned on with UseMC 1 and NMC 500.

A.6. Raw data of Monte Carlo

time delay[days]	probability
30.5613	0.054 704 7
31.3402	0.070 794 3
32.119	0.119 063
32.8979	0.189 858
33.6767	0.205 947
34.4556	0.186 64
35.2344	0.160 896
36.0133	0.112 627
36.7921	0.074 012 3
37.5709	0.022 525 5
38.3498	0.054 704 7
39.1286	0.016 089 6
39.9075	0.006 435 85
40.6863	0.003 217 92
41.4652	0
42.244	0.003 217 92
43.0229	0
43.8017	0
44.5806	0.003 217 92
45.3594	0

Table A.3.: Output of Monte Carlo method

A.7. Raw data for dark current part

filename	mean	sigma
DARK_-10deg_30s.fits	1941.24	8.86
DARK_-10deg_60s.fits	1941.63	8.86
DARK_-10deg_120s.fits	1942.73	8.22
DARK_-2deg_30s.fits	1938.75	8.86
DARK_-2deg_60s.fits	1940.01	8.86
DARK_-2deg_120s.fits	1943.21	8.43
DARK_-4deg_30s.fits	1938.97	7.83
DARK_-4deg_60s.fits	1939.86	8.97
DARK_-4deg_120s.fits	1942.14	9.07
DARK_-6deg_30s.fits	1939.16	8.61
DARK_-6deg_60s.fits	1940.33	8.02
DARK_-6deg_120s.fits	1941.88	9.07
DARK_-8deg_30s.fits	1939.73	8.22
DARK_-8deg_60s.fits	1940.93	9.18
DARK_-8deg_120s.fits	1942.00	8.12
DARK_0deg_30s.fits	1938.49	8.43
DARK_0deg_60s.fits	1940.75	9.29
DARK_0deg_120s.fits	1944.34	9.71
DARK_2deg_30s.fits	1938.98	8.97
DARK_2deg_60s.fits	1941.85	8.97
DARK_2deg_120s.fits	1946.73	9.29
DARK_4deg_30s.fits	1939.49	9.61
DARK_4deg_60s.fits	1943.43	9.37
DARK_4deg_120s.fits	1949.80	9.71
DARK_6deg_30s.fits	1941.53	9.07
DARK_6deg_60s.fits	1946.10	9.71
DARK_6deg_120s.fits	1955.05	9.37
DARK_8deg_30s.fits	1943.90	9.29
DARK_8deg_60s.fits	1950.09	10.29
DARK_8deg_120s.fits	1962.59	9.96
DARK_10deg_30s.fits	1951.54	9.48
DARK_10deg_60s.fits	1956.02	9.25
DARK_10deg_120s.fits	1971.66	10.27

A.8. Raw data for dark current fitting

temperature	slope	sigma slope	intercept	sigma intercept
-1.000×10^{1}	1.685×10^{-2}	1.270×10^{-3}	1.941×10^{3}	1.040×10^{-1}
-2.000	5.015×10^{-2}	2.733×10^{-3}	1.937×10^{3}	2.216×10^{-1}
-4.000	3.544×10^{-2}	2.042×10^{-3}	1.938×10^{3}	1.546×10^{-1}
-6.000	2.962×10^{-2}	3.495×10^{-3}	1.938×10^{3}	2.685×10^{-1}
-8.000	2.429×10^{-2}	5.076×10^{-3}	1.939×10^{3}	4.111×10^{-1}
0.000	6.457×10^{-2}	3.886×10^{-3}	1.937×10^{3}	2.937×10^{-1}
2.000	8.548×10^{-2}	3.613×10^{-3}	1.937×10^{3}	2.825×10^{-1}
4.000	1.133×10^{-1}	6.359×10^{-3}	1.936×10^{3}	5.007×10^{-1}
6.000	1.501×10^{-1}	7.633×10^{-4}	1.937×10^{3}	6.030×10^{-2}
8.000	2.077×10^{-1}	4.807×10^{-4}	1.938×10^{3}	3.753×10^{-2}
1.000×10^{1}	2.280×10^{-1}	2.918×10^{-2}	1.944×10^{3}	2.230

A.9. Raw data for detector system "gain" part

filename	mean	sigma
`BIAS.fit`	1954.540	9.830
`difference.fit`	15.700	205.260
`FLAT-1.fit`	31 735.080	251.770
`FLAT.fit`	31 750.790	239.940

A.10. Raw data for detector linearity part

filename	mean	sigma
FLATLIN_0.15s-1.fits	11 220.250	88.600
FLATLIN_0.15s_diff.fits	−59.520	117.310
FLATLIN_0.15s.fits	11 160.730	90.730
FLATLIN_0.3s-1.fits	20 498.220	135.990
FLATLIN_0.3s_diff.fits	18.590	163.170
FLATLIN_0.3s.fits	20 516.810	133.010
FLATLIN_0.4s-1.fits	26 596.400	155.640
FLATLIN_0.4s_diff.fits	23.150	188.270
FLATLIN_0.4s.fits	26 619.550	160.650
FLATLIN_0.5s-1.fits	32 741.970	188.300
FLATLIN_0.5s_diff.fits	−73.750	213.710
FLATLIN_0.5s.fits	32 668.220	187.540
FLATLIN_0.7s-1.fits	44 998.170	243.280
FLATLIN_0.7s_diff.fits	−3.700	239.980
FLATLIN_0.7s.fits	44 994.460	231.830
FLATLIN_0.85s-1.fits	54 057.690	275.730
FLATLIN_0.85s_diff.fits	12.140	275.230
FLATLIN_0.85s.fits	54 069.830	273.180
FLATLIN_0.8s-1.fits	50 990.730	257.050
FLATLIN_0.8s_diff.fits	83.810	259.150
FLATLIN_0.8s.fits	51 074.540	260.030
FLATLIN_0.95s-1.fits	60 173.400	297.390
FLATLIN_0.95s_diff.fits	−244.090	287.330
FLATLIN_0.95s.fits	59 929.310	287.210
FLATLIN_0.9s-1.fits	57 056.050	273.540
FLATLIN_0.9s_diff.fits	−214.050	269.480
FLATLIN_0.9s.fits	56 842.000	279.760
FLATLIN_1.05s-1.fits	65 533.480	0.000
FLATLIN_1.05s_diff.fits	−0.380	0.000
FLATLIN_1.05s.fits	65 533.100	0.000
FLATLIN_1.0s-1.fits	62 954.810	302.630
FLATLIN_1.0s_diff.fits	−42.820	291.420
FLATLIN_1.0s.fits	62 911.990	303.450
FLATLIN_1.15s-1.fits	65 535.000	0.000
FLATLIN_1.15s_diff.fits	0.000	0.000
FLATLIN_1.15s.fits	65 535.000	0.000
FLATLIN_1.1s-1.fits	65 535.000	0.000
FLATLIN_1.1s_diff.fits	0.000	0.000
FLATLIN_1.1s.fits	65 535.000	0.000
FLATLIN_1.25s-1.fits	65 535.000	0.000
FLATLIN_1.25s_diff.fits	0.000	0.000
FLATLIN_1.25s.fits	65 535.000	0.000
FLATLIN_1.2s-1.fits	65 535.000	0.000
FLATLIN_1.2s_diff.fits	0.000	0.000
FLATLIN_1.2s.fits	65 535.000	0.000
FLATLIN_1.3s-1.fits	65 535.000	0.000
FLATLIN_1.3s_diff.fits	0.000	0.000
FLATLIN_1.3s.fits	65 535.000	0.000

Bibliography

[1] VALERY A GORBUNOV DMITRY S. RUBAKOV. *INTRODUCTION TO THE THEORY OF THE EARLY UNIVERSE: hot big bang theory*. WS PROFESSIONAL, 2017.

[2] Edward W. Kolb and Michael S. Turner. *The Early Universe*. Addison-Wesley, 1993.

[3] Unknown. *Advanced lab course in physics at Bonn University: Optical Astronomy and Gravitational Lensing*. 2020.

[4] P. Schneider. *Introduction to Gravitational Lensing and Cosmology*.

[5] Chien Y. Peng. *GALFIT USER'S MANUAL*. URL: https://users.obs.carnegiescience.edu/peng/work/galfit/README.pdf.

[6] C. Vuissoz et al. "COSMOGRAIL: the COSmological MOnitoringof GRAvItational Lenses". In: (2006).

[7] Planck Collaboration et al. *Planck 2015 results. XIII. Cosmological parameters*. 2015. arXiv: 1502.01589 [astro-ph.CO].

[8] Robert J J Grand et al. "The effects of dynamical substructure on Milky Way mass estimates from the high-velocity tail of the local stellar halo". In: *Monthly Notices of the Royal Astronomical Society: Letters* 487.1 (June 2019), pp. L72–L76. ISSN: 1745-3933. DOI: 10.1093/mnrasl/slz092. URL: http://dx.doi.org/10.1093/mnrasl/slz092.

[9] N. Aghanim et al. "Planck 2018 results. VI. Cosmological parameters". In: *Astron. Astrophys.* 641 (2020), A6. DOI: 10.1051/0004-6361/201833910. arXiv: 1807.06209 [astro-ph.CO].

[10] Adam G. Riess et al. "Large Magellanic Cloud Cepheid Standards Provide a 1% Foundation for the Determination of the Hubble Constant and Stronger Evidence for Physics beyond ΛCDM". In: *Astrophys. J.* 876.1 (2019), p. 85. DOI: 10.3847/1538-4357/ab1422. arXiv: 1903.07603 [astro-ph.CO].

[11] Nicholas D. Morgan, Jeffrey A. Snyder, and Louis H. Reens. "SDSS 1650+4251: A New gravitational lens". In: *Astron. J.* 126 (2003), p. 2145. DOI: 10.1086/378602. arXiv: astro-ph/0305036.

[12] SBIG astronomical instruments. *STL-6303E Typical specifications*. URL: https://www.virtualtelescope.eu/wordpress/wp-content/uploads/2012/10/STL6303_specs_7.12.11.pdf.